Molecular and Cellular Biochemistry (2025) 480:3647–3668
https://doi.org/10.1007/s11010-024-05194-8

PSAT1 promotes the progression of colorectal cancer by regulating Hippo-YAP/TAZ-ID1 axis via AMOT

Minshan Tang[1,2] · Kai Song[1,2] · Danning Xie[1,2] · Xinyu Yuan[1,2] · Yaxuan Wang[1,2] · Zhiyang Li[1,2] · Xiansheng Lu[1,2] · Liang Guo[1,2] · Xiaotong Zhu[1,2] · Le Xiong[1,2] · Wenqian Zhou[1,2] · Jie Lin[1,2]

Received: 13 August 2024 / Accepted: 14 December 2024 / Published online: 31 December 2024

Abstract

Colorectal cancer (CRC) ranks third for morbidity and second for mortality among all digestive malignant tumors worldwide, but its pathogenesis remains not entirely clear. Bioinformatic analyses were performed to find out important biomarkers for CRC. For validation, reverse transcription-quantitative PCR, western blotting, and immunohistochemistry were performed. Then, cell transfection, gain- and loss-of-function assays, immunofluorescence, cell line RNA-sequencing and analyses, and in vivo tumorigenesis assay were also performed to further explore the mechanism. We prioritized phosphoserine aminotransferase 1 (PSAT1) as an important biomarker in CRC. PSAT1 expression was gradually up-regulated as the CRC disease progresses and may relate to poor prognosis. PSAT1 promoted the malignant behaviors of CRC cells. Although PSAT1 is an enzyme essential to serine biosynthesis, an exogenous supplement of serine did not completely rescue the malignant behaviors in PSAT1-knockdown CRC cells. Interestingly, PSAT1 inhibited the Hippo tumor-suppressor pathway by promoting the nucleus-localization of YAP/TAZ and increasing the expression of ID1 in CRC cells. Furthermore, AMOT, a vascular-related molecule that molecularly interacts with YAP/TAZ, was up-regulated upon PSAT1 knockdown in CRC cells. Knocking down AMOT partially rescued the inhibition of proliferation and the reduced nuclear localization of YAP/TAZ caused by PSAT1 knockdown in CRC cells. Moreover, PSAT1 was closely related to vascular-related pathways, in which AMOT might act as a mediator. Finally, PSAT1 promoted CRC proliferation by negatively regulating AMOT in vivo. PSAT1 could enhance the progression of colorectal cancer by regulating Hippo-YAP/TAZ-ID1 axis via AMOT, which is independent of the metabolic function of PSAT1.

Keywords Colorectal cancer · PSAT1 · Serine synthesis · AMOT · Hippo pathway · Tumor progression

Introduction

Colorectal cancer (CRC) stands as one of the most prevalent malignant tumors within the digestive system. Globally, CRC holds the third position in terms of morbidity and the second for mortality, highlighting its significant impact on public health [1]. For those battling advanced-stage colorectal cancer (CRC), the 5-years survival rate hovers under 15%, largely attributed to the spread of the disease through metastasis [2]. Therefore, it is imperative to identify tumor targets and further explore the molecular mechanism behind the rapid progression of CRC, giving new insights into the screening and therapeutic strategies for the malignancy.

This study aims to look for genes whose expression levels gradually up-regulate as the CRC disease progresses and are significantly different from that of normal colorectal tissue since the early stage of CRC. These genes are worthy of study because they may be involved throughout the entire process of CRC occurrence, development, and metastasis. Phosphoserine aminotransferase 1 (PSAT1) is selected as the research biomarker based on the CRC datasets. PSAT1 is currently known as a key enzyme in the second step of de novo serine synthesis pathway(SSP) [3]. An increasing number of proof show that metabolic reprogramming is critical to carcinoma progression [4–6]. Among them, an important metabolic reprogramming issue is the SSP [3].

✉ Jie Lin
jielin_gz@126.com

[1] Department of Pathology, Nanfang Hospital, School of Basic Medical Sciences, Southern Medical University, Guangzhou 510515, Guangdong, China

[2] Guangdong Province Key Laboratory of Molecular Tumor Pathology, Guangzhou 510515, Guangdong, China

PSAT1 integrates metabolic pathways such as pathways for SSP, citric acid cycle, one-carbon metabolism, nucleic acid biosynthesis, and glycolysis, and these pathways are of great importance to cell proliferation, migration, and so on [7, 8]. PSAT1 has been reported to promote cancer progression in some tumors [7, 9–15] and at least serve as a metabolic enzyme in multiple tumor processes [7, 10, 12, 16]. However, the non-metabolic moonlighting roles of PSAT1 in diverse tumors are still rarely studied [15, 17, 18]. Whether PSAT1 has an enzymatic-independent role in tumors remains largely unclear.

The Hippo tumor-suppressor pathway, which involves the regulation of differentiation and proliferation in cells, has been a great deal of attention in cancer research in the past decade [19]. Upon the activation of the Hippo pathway, the kinase complex LATS1/2-Mob1 causes the phosphorylation of YAP/TAZ, which affects the subcellular distribution and stability of the YAP/TAZ complex, a master regulator in cancer [20–22]. However, YAP/TAZ, which acts as an oncogenic module in the Hippo pathway [19], is also regulated in other ways [22], but the molecular insight remains limited.

AMOT has been confirmed to molecularly interact with YAP/TAZ, which is separate from the kinase activity of LATS1/2-Mob1 [20], suggesting that AMOT may affect the downstream impact of Hippo pathways through YAP/TAZ. AMOT is a member of the angiostatin-binding Motin protein family. It may negatively regulate the influence of angiostatin on angiogenesis and be correlated with the migratory behavior of endothelial cells during vascularization [23]. Two isoforms are known for AMOT: p80 and p130. Amot-p80 is instrumental in the regulation of vascular morphogenesis and the migratory behavior of endothelial cells, and Amot-p130 is significant to controlling cell shape [23, 24]. Research on malignancies such as lung carcinoma and diffuse large B cell lymphoma (DLBCL) indicated that AMOT or its specific isoforms serve as a tumor suppressor [25–31], while in some other malignancies including CRC, AMOT or its specific isoforms were identified as a tumor promoter [23, 32–35]. However, the upstream regulator of AMOT and the role of AMOT in tumors are not fully clarified.

Hence, in CRC progression, we emphasize the new findings of a non-metabolic moonlighting character for PSAT1 and elucidate the potential mechanism that entails AMOT, a vascular-related molecule.

Materials and methods

Tissue samples and cell lines

This study was based on the following research samples: Fresh primary CRC lesions and paired normal colorectal mucosal tissue from 15 CRC patients; and paraffin sections collected from 129 CRC patients (68 men and 61 women) between 2018 and 2022, including 129 primary CRC lesions, 129 paired normal colorectal mucosal tissue, 39 paired regional LN metastases, and 23 paired liver metastases. All patients were informed of the research and signed informed consent forms. The acquisition of clinical and pathological information of all patients was approved by the Medical Ethics Committee of Nanfang Hospital, Southern Medical University, China. All patients were diagnosed with primary colorectal cancer by two pathologists, and no chemotherapy or radiotherapy was given before the resection of the primary lesions and metastases. All the cases with metastasis were diagnosed with metastatic diseases by pathology or imaging after they underwent the first CRC tumor resection surgery during hospitalization.

The normal colonic epithelial cell line FHC, eight human CRC cell lines, including HT29, LoVo, DLD-1, LS 174 T, RKO, Caco-2, SW480, HCT-15, HCT116, and SW620 were obtained from the American Type Culture Collection (ATCC) by our laboratory. All cell lines were cultivated in a complete growth medium within a cell culture incubator, maintained at a temperature of 37 °C, and an atmospheric condition of 5% CO2. In particular, the complete culture medium for FHC was prepared according to a formulation from ATCC, the Caco-2 cell line was cultured in RPMI-1640 Medium (Gibco, from the US) with 20% fetal bovine serum (FBS) (Gibco, from the US). In addition, other cell lines were maintained in RPMI-1640 Medium but adjusted to 10% FBS concentration.

RNA extraction, RT-PCR, and qPCR

For each CRC cell line, total RNA was isolated from each colorectal cancer (CRC) cell line via the phenol/chloroform extraction technique, and subsequently, the RNA samples were converted into cDNA through reverse transcription with the Evo M-MLV RT Master MIX kit (AG11706). qPCR was performed using SYBR® Green Pro Taq HS premixed qPCR kit (including Rox) (AG11718) in the ABI 7500 Fast Real-Time PCR System. Information about primer sequences in our research is offered in Supplementary Table S1. Each experiment was conducted in triplicate, and the internal reference gene was GAPDH.

WB and antibodies

Cell samples were lysed on ice with RIPA lysis buffer (high strength) (Hangzhou FUDE Biotechnology), and protein samples were separated by electrophoresis in 10% SDS-PAGE gels and transferred to PVDF membranes (0.45 μm, IPVH00010, Merck Millipore). The PVDF membranes were pre-treated by immersing them in a 5% skim milk solution for 1 h at ambient temperature. Subsequently, the

membranes were incubated with the primary antibodies for a period ranging from 12 to 16 h at 4 °C. The membrane was further processed by incubating it with the HRP-conjugated secondary antibodies for 1 h at ambient temperature. Ultimately, the detection of signal density was achieved through chemiluminescence with the application of an ultra-sensitive ECL luminescent reagent (Biosharp Technology). Information about primary antibodies and secondary antibodies in our research is offered in Supplementary Table S2.

Immunohistochemistry

Immunohistochemistry (IHC) was performed manually according to antibody manufacturer instructions. The optimal IHC protocol was determined through a preliminary experiment where liver and kidney tissue sections incubated with anti-PSAT1 were used as positive controls, tissue sections incubated with PBS rather than antibody were used as negative controls, various combinations of concentration and incubation time were tried, and staining intensity was evaluated under a microscope. Subsequently in the formal experiment, sections were directly stained with DAB reagent (ZLI-9018, ZSGB-BIO), scored, and photographed, and for each batch of tissue sections, both positive and negative controls were included. Information about antibodies used in IHC in our research is offered in Supplementary Table S2.

The total IHC score was counted as the sum of the staining intensity and the positive area percentage in tumor cells. The positive area percentage (denoted by S) was scored from 0 to 4: 0 for negative, 1 for $0 < S \leq 25\%$, 2 for $25\% < S \leq 50\%$, 3 for $50\% < S \leq 75\%$, and 4 for $S > 75\%$. The classification of staining intensity was divided into four distinct levels: 0 indicated the absence of staining, 1 represented poor staining, 2 denoted moderate staining, and 3 corresponded to intense staining. We set half of the highest theoretical total score as the cut-off point. Samples exhibiting a total PSAT1 score exceeding 3.5 were categorized as having high expression, whereas those with scores at or below 3.5 were considered to have low expression.

Cell transfection

PSAT1 over-expressing (EX-V0307-Lv201), the corresponding mock, shPSAT1 (sh1- sh4), and scrambled shRNA (sh-NC) vector plasmids were purchased from Guangzhou iGene Biotechnology Limited company. To ensure a high overexpression efficiency, the CMV promoter of the overexpression plasmid was replaced by an EF-1α promoter, the eGFP tag of the plasmid was removed, and such editing was validated by Sanger sequencing. Stable over-expression and knockdown of PSAT1 were performed by the psPAX2/pMD2.G lentiviral delivery system with the above-mentioned vectors and HEK293-FT cells. PSAT1-overexpressed DLD-1, SW480, and RKO cell lines, and PSAT1-knockdown HCT-15, DLD-1, and SW480 cell lines were constructed, while the corresponding cell lines transduced with the mock lentiviral vector or the sh-NC vector were used as a negative control in PSAT1 over-expression or PSAT1 knockdown experiments, respectively. Recombinant lentiviruses were produced in HEK293-FT cells by polyethyleneimine (PEI) when we conducted transient transfection, and were used to transfect the indicated cells with polybrene (10 μg/mL). The lentivirus-transfected cells were selected using puromycin (1–5 μg/mL, according to cell line-specific sensitivity measured in a pre-experiment) for 6 days preceded validation. The siRNA targeting AMOT and the control scrambled siRNA were purchased from GenePharma, and cells were transfected with 50 nM of siRNA and lipofectamine 2000 (5 μl/well for 6-well plates). The over-expression and knockdown efficiency of the transfected cells were validated using Reverse transcription-quantitative PCR (RT-qPCR) and Western blotting. Information about siRNAs of AMOT, shPSAT1(sh1—sh4) plasmids, and the PSAT1 over-expressing plasmid is provided in Supplementary Table S3 and Supplementary Table S4.

Cell proliferation assays

During the CCK-8 assay, cells to be treated were plated in 96-well plates in 3–5 replicates at 1500 cells/well for 24 h, 48 h, 72 h, 96 h, and 120 h. During the periods, the medium needed to be replaced with fresh medium as required. At the required time point, the diluted CCK-8 solution, with the volume of CCK-8 reagent (Yeasen) being 10% of the volume of the culture medium, was prepared for each well, the complete culture medium was aspirated, and then a volume of 100 μl of CCK-8 solution was dispensed into each well. Then, the cells were cultured in the dark for 2 h. The optical density (OD) in each well was determined at a wavelength of 450 nm.

In the clonogenic assay, cells were seeded in 6-well plates at 500 or 1000 cells/well depending on the growth rate of the different cell lines, with 3 replicate wells per group in each independent assay. During the assay, the medium needed to be replaced with fresh medium as required. Subsequently, the cells were treated with a 4% paraformaldehyde solution for fixation, after which they were stained using crystal violet. The ImageJ software was used to set parameters and count the number of colonies. Each assay was repeated three times.

Transwell migration and invasion assays

Transwell chambers (8 μm pore size, Corning, NY, US) were used to observe cell migration and invasion. According to the growth rate of different cell lines, 1×10^5 or 2×10^5 cells

were mixed with 200 µl serum-free medium and placed in a chamber, and 500 µl RPMI-1640 Medium with 20% FBS was added to the lower chamber, that is, the well of the 24-well plate, with 3 replicate wells per group in each independent assay. In an invasion assay, 100 µl matrigel matrix (Corning, US) diluted 1:8 was added to the upper chamber and placed in the 37℃ incubator for 2–3 h before cell inoculation. After the corresponding time was reached, cells were covered in 4% paraformaldehyde, after which they were stained using crystal violet, and quantified the cell count passing through the apertures in five selected areas (×200) at random by a light microscope. Each assay was performed in three times.

The migration and invasion assays with serine added were basically the same as the preceding migration and invasion assays, but the cells of the experimental group where serine was added needed to be cultured in the complete medium with a final 12 mM concentration of L-serine (HY-N0650, MCE) for three days before the migration and invasion assays. During the assays, L-serine (HY-N0650, MCE) must be added to the upper and lower chambers at the same time to reach the final medium concentration of 12 mM.

Flow cytometry for apoptosis detection and cell cycle detection

The Annexin V-APC/PI fluorescence double-staining apoptosis detection kit (E-CK-A217, Elabscience) and cell cycle detection (also called DNA content measurement) kit (E-CK-A351, Elabscience) were used for apoptosis and cell cycle detection, respectively, according to the manufacturer's instructions. The apoptosis and cell cycle were detected using a flow cytometer, and analysis was conducted using the FlowJo software. Three replicate wells were set up for each assay and each assay was conducted in three times.

Immunofluorescence assay

Cells were uniformly distributed onto confocal dishes at a seeding density of 1×10^4 cells per well and then incubated in a cell culture incubator for 24 h. Then, the culture medium was aspirated and subsequently replaced with PBS to rinse the cells. Following this, the cellular membranes were permeabilized using Triton X-100. The cells were incubated with primary antibodies TAZ at a 1:50 dilution ratio (anti-rabbit, A8202, Abclonal) and YAP1 at a 1:200 dilution ratio (anti-mouse, 66,900–1, Proteintech) overnight at 4 °C. Subsequently, primary antibodies were washed away with PBS again, and the cells were incubated using Dylight649-conjugated goat anti-mouse IgG (H + L) (E032610-01, EarthOx) and Dylight549-conjugated goat anti-rabbit IgG (H + L) (E032320-01, EarthOx) at 1:100 dilution ratio at ambient temperature in a dark chamber for 1 h. Subsequently, the cells were counterstained with 4′,6-diamidino-2-phenylindole (DAPI, Sigma, MO), and then images were captured using a Zeiss laser scanning confocal microscope (ZEISS, LSM 880, Germany).

In vivo tumorigenesis assay

Four-week-old male BALB/c-nu mice were procured from Spefford (Beijing) Biotechnology Co., Ltd., quarantined, and raised in the SPF barrier environment of the Experimental Animal Center of Guangzhou Southern Medical University. DLD-1 sh-NC and sh-PSAT1-2 cells were prepared, digested, and counted, then resuspended in PBS, and transported on ice. 200 µl of cell suspension was injected subcutaneously into each mouse (1×10^7 cells/mouse). Since the day when the tumor can be palpated, the tumor-bearing size of each mouse was measured every 2–3 days and the tumor volume was calculated according to the formula: $\text{Volume} = 1/2 \times (\text{Width}^2 \times \text{Length})$. At the end of the observation period, the mice were subjected to humane euthanasia. Subsequently, the xenografted tumors were meticulously excised, documented via photographic means, and preserved in formalin for HE and IHC detection. All experimental procedures complied with protocols admitted by the Institutional Animal Care And Use Committee (IACUC) and the Experimental Animal Ethics Committee of Southern Medical University in Guangzhou, China (SMUL2023081).

Analysis of differentially expressed genes

The gene expression microarray datasets GSE41657 and GSE74602 were retrieved from the Gene Expression Omnibus website (https://www.ncbi.nlm.nih.gov/geo/), and the RNA-sequencing read count matrix of TCGA-COADREAD was downloaded from the UCSC Xena data-hub (https://xenabrowser.net/datapages/). For microarray datasets, DEGs were analyzed by the Limma package. For the TCGA-COADREAD data and our CRC cell line RNA-sequencing data, DEGs were analyzed by the Limma-voom approach. For public datasets, the criteria for DEGs are as follows: the absolute value of logFC should be larger than 2 and the adjusted_p value should be less than 0.05. For CRC cell line RNA-sequencing, the DEGs criteria are as follows: $|\text{logFC}| > 1$ and adjusted_$p < 0.05$, and only the genes met the criteria and showed the same directions of expression change in the 2 shPSAT1 groups were defined as DEGs upon PSAT1 knockdown.

Time series clustering of genes

Starting from the GSE41657 expression matrix, first according to the aforementioned differentially expressed gene analysis method, genes that were differentially expressed

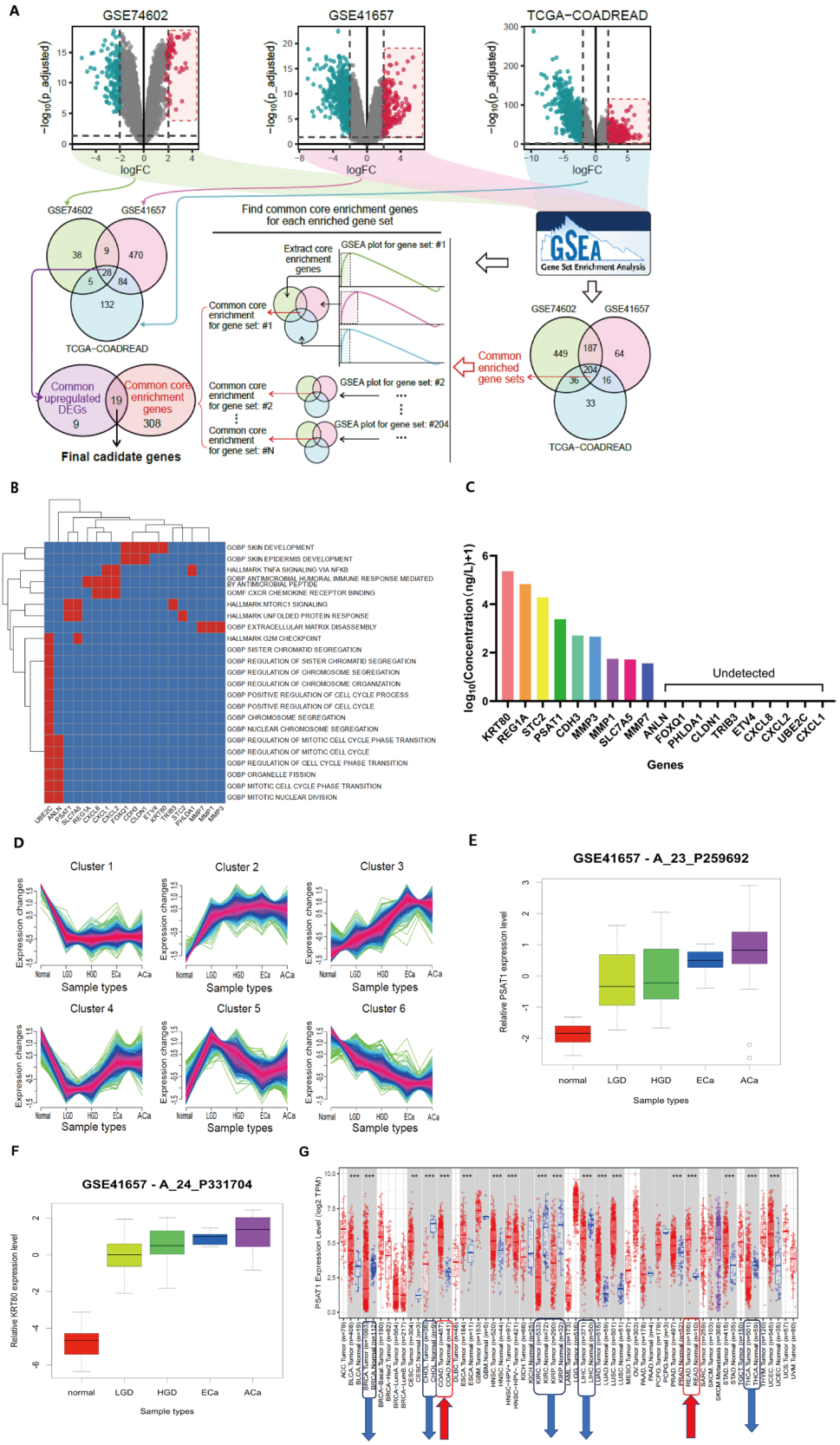

Fig. 1 Preliminary bioinformatics analysis of public datasets identified key biomarkers of CRC. **A** Flow chart, showing the screening process of final candidate genes. Venn diagram and flowchart of preliminary bioinformatics analysis of GEO and ATCC public databases. The differentially expressed genes meet |log2FC|> 2 and adjusted_p < 0.05. **B** Heat map about 19 intersecting genes (**A**) which could all be enriched in the same gene set in GSE74602, TCGA-COADREAD, and GSE41657 colorectal cancer data sets. **C** Histograms of the plasma protein concentrations of the protein products of the 19 genes, the intersection in (**A**). The proteomics results measured based on mass spectrometry analysis are provided by the HPA website. **D** Time series analysis of the GSE41657 dataset. **E, F** Box plots of the chip expressions of PSAT1 (**E**) and KRT80 (**F**) at the stages of normal tissue, low-grade colorectal adenoma, high-grade colorectal adenoma, early-stage cancer, and advanced cancer. The data source is the GSE41657 dataset. **G** Box plot of the analysis carried out based on the TCGA database on the TIMER website. The red arrow marks the dataset of colon cancer and rectal cancer, and the blue arrow marks the dataset of cancers in which the expression level of PSAT1 in normal tissue is higher than that in cancer

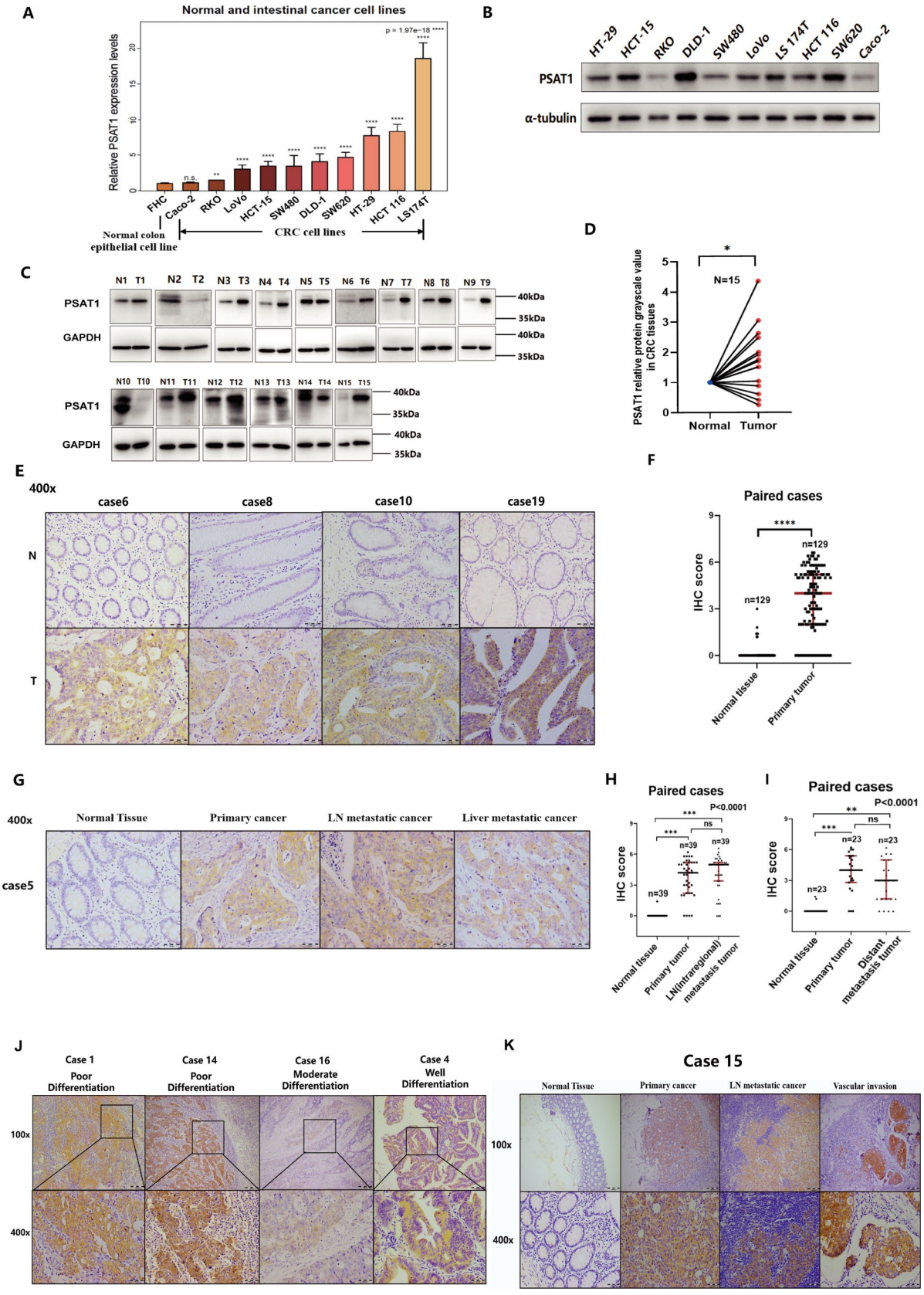
A
Normal and intestinal cancer cell lines
Relative PSAT1 expression levels
p = 1.97e−18 ****
FHC
Caco-2
RKO
LoVo
HCT-15
SW480
DLD-1
SW620
HT-29
HCT 116
LS174T
Normal colon epithelial cell line
CRC cell lines
B
HT-29
HCT-15
RKO
DLD-1
SW480
LoVo
LS 174T
HCT 116
SW620
Caco-2
PSAT1
α-tubulin
C
PSAT1
GAPDH
40kDa
35kDa
D
PSAT1 relative protein grayscale value in CRC tissues
N=15
Normal
Tumor
E
400x
case6
case8
case10
case19
N
T
F
Paired cases
IHC score
n=129
Normal tissue
Primary tumor
G
400x
Normal Tissue
Primary cancer
LN metastatic cancer
Liver metastatic cancer
case5
H
Paired cases
P<0.0001
IHC score
n=39
Normal tissue
Primary tumor
LN(intraregional) metastasis tumor
I
Paired cases
P<0.0001
IHC score
n=23
Normal tissue
Primary tumor
Distant metastasis tumor
J
Case 1 Poor Differentiation
Case 14 Poor Differentiation
Case 16 Moderate Differentiation
Case 4 Well Differentiation
100x
400x
K
Case 15
Normal Tissue
Primary cancer
LN metastatic cancer
Vascular invasion
100x
400x

◂**Fig. 2** Expression levels of phosphoserine aminotransferase 1(PSAT1) in Colorectal cancer (CRC). **A** PSAT1 mRNA expression levels in normal colon epithelial cell line FHC and CRC cell lines by Reverse transcription-quantitative PCR(RT-qPCR) assay. **B** PSAT1 protein expression levels in human CRC cell lines by Western Blot(WB) assay. **C** WB showed the PSAT1 protein expression levels of fresh human CRC tissue and normal colorectal mucosal tissue. **D** Paired line scatter plot. Comparing the relative protein expression grayscale values of PSAT1 in (**C**). **E, F** Representative immunohistochemical (IHC) images (**E**) and scatter plots (**F**) of PSAT1 expression levels of paired normal colorectal mucosal tissue and CRC tissue from 129 patients. **G–I** Representative IHC images (**G**) and scatter plots (**H, I**) of PSAT1 expression levels of paired normal colorectal mucosal tissue, primary CRC lesions, regional LN metastases, and liver metastases. **J** Representative IHC images of PSAT1 expression levels in CRC cases with varying degrees of differentiation. **K** Representative cases of IHC sections: PSAT1 expression levels in completely paired normal colorectal mucosal tissue, primary CRC lesions, regional LN metastases, and cancer nests within vessels. "ns" denotes no statistically significant difference; * indicates $p < 0.05$; ** signify $p < 0.01$; *** are used for $p < 0.001$; **** correspond to $p < 0.0001$

between the control group and at least one of the adenoma or carcinoma group were identified as candidates using adjusted_$p < 0.05$ as a threshold. Then, the candidate genes were soft-clustering according to their time-course expression patterns through groups of normal epithelial tissue, adenoma, and carcinoma using the Mfuzz package (version 2.60.0).

Gene Set Enrichment Analysis (GSEA) and Gene Set Variation Analysis (GSVA)

To infer the biological function of PSAT1 in CRC, first, genes from the expression matrix were sorted on the Spearman correlation coefficient of their expression levels with that of PSAT1. Then, GSEA was performed by the clusterProfiler package (version 4.7.1.003) on the sorted gene list and the gene set list MSigDB v2022.1.Hs retrieved from Molecular Signature Database (MSigDB, https://www.gsea-msigdb.org/gsea/msigdb/), the significantly enriched gene sets were defined as those with p value less than 0.05 and false discovery rate (FDR) less than 0.25 in GSEA. Specifically for the CRC cell line RNA-sequencing, only the gene sets that met the above criteria and shared the same enrichment directions (determined by signs of the enrichment score) in the 2 shPSAT1 groups were defined as significantly enriched ones. The corresponding heat maps showing the top 40 or all common core enrichment genes. Gene in the heat maps are arranged in a descending order according to their logFC values.

GSVA was performed (GSVA package version 1.44.5) with the MSigDB v2022.1.Hs gene sets, which resulted in GSVA scores of the gene sets. Then for each gene set, the correlation between the GSVA score and PSAT1 expression levels among samples was assessed using Spearman correlation analyses. The filter criteria are |Spearman rho| ≥ 0.2, p value < 0.05, p adjust < 0.05.

CRC biomarker prioritization

First, we analyzed DEGs between CRC tissue and normal tissue of three public datasets, GSE41657, GSE74602, and TCGA-COADREAD. We obtained 28 candidate genes that were jointly up-regulated in the datasets. Next, to prioritize the genes for biological functions, gene set enrichment analyses (GSEA) were performed on the three datasets, and we defined the gene sets that were enriched in the tumor side in all the datasets as the common enriched gene sets. For each of the gene sets, we collected the genes that were identified by the GSEA algorithm as "core enrichment" in the three datasets, and there were 19 such "common core enrichment" genes in total. Then, to prioritize potential plasma biomarkers, we compared protein abundance of these genes in plasma detected by mass spectrometry from the Human Protein Atlas (HPA) website (https://www.proteinatlas.org/) and we showed that only nine of them are detected in plasma: KRT80, REG1, STC2, PSAT1, CDH3, MMP3, MMP1, SLC7A5, and MMP7. Finally, by time-series gene expression analysis of the GSE41657 dataset, we found that the expression levels of PSAT1, KRT80, SLC7A5, MMP1, and MMP7 gradually increased as the disease progressed from the normal, adenoma, to the CRC period. However, only PSAT1 and KRT80 showed plasma protein concentration above 1 μg/L. Specifically, we chose PSAT1, a key enzyme of serine metabolism, for further verification and exploring, as there is increasing concern in recent literature about the metabolic and non-metabolic involvement of metabolic enzymes in cancers.

RNA-sequencing and analysis of CRC cell lines

The cell samples were lysed by RNAex Pro Reagent according to the company's instructions and the extracted samples were collected and immediately sent to the company of Genega for mRNA purification, library construction, and sequencing. The sequencing platform was the BGI sequencing platform, the mode was double-ended PE150, and the sequencing data volume was 6G bases per sample. The sequencing off-machine data were quality-controlled and filtered using fastp (version 0.23.2) software to obtain clean reads. Then, we used RSEM (version 1.3.1) calling the alignment tool STAR (version 2.7.0d) to align the clean reads to the hg38 reference, and estimated transcript and gene abundance based on the expectation maximization (EM) algorithm, which finally resulted in the gene-read-counts matrix and the Fragments Per Kilobase of exon model per Million mapped fragments (FPKM) expression matrix.

Table 1 Relationship between PSAT1 immunoreactivity and clinicopathologic features in patients with CRC

Characteristic	All cases ($n=129$)	PSAT1 immunoreactivity		*P* value
		Low expression ($n=58$) (%)	High expression ($n=71$) (%)	
Gender				0.880
Male	68	31 (45.6)	37 (54.4)	
Female	61	27 (44.3)	34 (55.7)	
Age(yrs)				0.182
≤60	55	21 (38.2)	34 (61.8)	
>60	74	37 (50.0)	37 (50.0)	
Differentiation				0.003
Well + Moderate	100	52 (52.0)	48 (48.0)	
Poor	29	6 (20.7)	23 (79.3)	
T Classification				0.734
T1 + T2	33	14 (42.4)	19 (57.6)	
T3 + T4	96	44 (45.8)	52 (54.2)	
LN metastasis				0.756
Negative (N0)	67	31 (46.3)	36 (53.7)	
Positive (N1-N2)	62	27 (43.5)	35 (56.5)	
Distant metastasis				0.297
Negative (M0)	99	47 (47.5)	52 (52.5)	
Positive (M1)	30	11 (36.7)	19 (63.3)	
AJCC stage				0.473
I + II	60	29 (48.3)	31 (51.7)	
III + IV	69	29 (42.0)	40 (58.0)	
Vascular invasion				0.028
Negative	80	42 (52.5)	38 (47.5)	
Positive	49	16 (32.7)	33 (67.3)	
Nerve invasion				0.302
Negative	92	44 (47.8)	48 (52.2)	
Positive	37	14 (37.8)	23 (62.2)	
dMMR or not				0.185
Yes	9	2 (22.2)	7 (77.8)	
Not	120	56 (46.7)	64 (53.3)	

Statistical analysis methods

For quantitative data analysis, two independent samples t tests (two-tailed) were used to compare two groups of independent samples that satisfy normal distribution and homogeneity of variances, and one-way ANOVA or two-way ANOVA was used to analyze single-factor or two-factor comparisons between multiple groups of independent samples satisfying normal distribution and homogeneity of variances. For displaying the comparisons, the values of each group are summarized as mean ± standard deviation. Wilcoxon test or Friedman test was used to compare 2 paired samples or multiple paired samples with non-normally distributed differences, and the values of each group were summarized as median ± interquartile range. The chi-square test was used to analyze qualitative data. Spearman correlation analysis was performed to assess the correlation. All analyses were performed in SPSS 20.0 and GraphPad Prism 8.0 (except bioinformatic analyses explained above). *P* values < 0.05 were considered significant.

Results

PSAT1 was up-regulated and may related to poor prognosis in CRC

We first prioritized PSAT1 as an important biomarker for CRC using public CRC datasets, as the expression levels of PSAT1 were higher in CRC tissue than those in normal colon mucosa, and the gene is gradually up-regulated as the CRC disease progresses(Fig. 1A–F, detail listed in Methods). These suggested that PSAT1 is worthy of study because it may be involved throughout the entire process of CRC occurrence, development, and metastasis. In addition, according to the analysis on the TIMER website in view of the TCGA database, the expression levels of PSAT1 vary in various human tumors and its expression was up-regulated in most tumors (Fig. 1G).

PSAT1 mRNA expression levels were up-regulated in CRC cell lines as compared with normal colon epithelial cell lines (Fig. 2A). The PSAT1 protein expression level of CRC cell lines showed that PSAT1 was highly expressed in DLD-1, HCT-15, SW620, and LS 174 T, was lowly expressed in RKO, SW480, and Caco-2, and was moderately expressed in HT-29, Lovo, and HCT 116 (Fig. 2B). PSAT1 protein expression level was stronger in CRC tissue than that in paired normal colorectal mucosal tissue as indicated by the Western Blot (WB) assay (Fig. 2C, D). The expression of PSAT1 was significantly higher in the primary CRC lesions than that in paired normal colorectal mucosal tissue as suggested by the immunohistochemistry (IHC) assay (Fig. 2E, F). We further found that PSAT1 expression levels were also significantly stronger in the regional LN metastases and liver metastases than in normal colorectal tissue. However, no expression difference of PSAT1 was found among the primary CRC lesions, regional LN metastases, and liver metastases (Fig. 2G–I).

Interestingly, in the IHC sections, we found that the staining intensity of PSAT1 was significantly stronger in poorly differentiated CRC cases than in other differentiation levels (Fig. 2J). In addition, we discovered that PSAT1 expression level was higher in cancer nests within

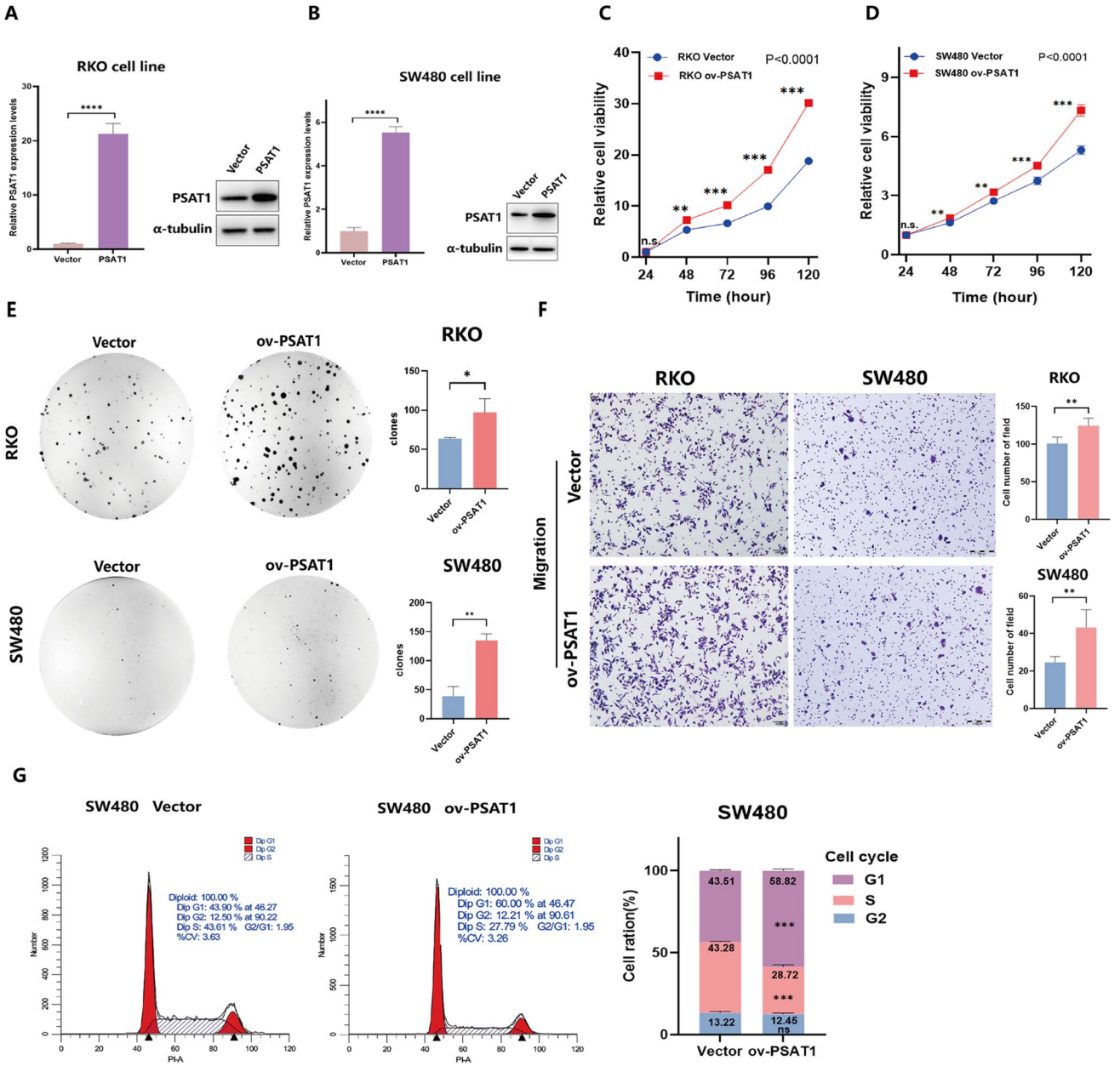

Fig. 3 Gain-of-function assays of PAST1 in CRC cells in vitro. **A, B** Verification of the efficiency of stable overexpression of PSAT1 in RKO (**A**), and SW480 cell lines (**B**) by WB and RT-qPCR assay. **C, D** CCK-8 assay, showing that overexpressing PSAT1 promoted the proliferation of RKO cells (**C**) and SW480 (**D**) cells in vitro. **E** Clonogenic assay, showing that overexpressing PSAT1 promoted the colony formation of RKO cells (on the upper part) and SW480 cells (on the lower part). **F** Transwell migration assay, showing that overexpressing PSAT1 promoted the migration of RKO cells and SW480 cells. **G** Cell cycle detection by flow cytometry, showing that overexpressing PSAT1 affected the cell cycle of SW480 cells and could induce arrest in the G1 phase. "ns" denotes no statistically significant difference; * indicates $p < 0.05$; ** signify $p < 0.01$; *** are used for $p < 0.001$; **** correspond to $p < 0.0001$

the vessel than in the primary lesions and metastases (Fig. 2K). We further analyzed the clinicopathological parameters of 129 patients, and the analysis results reveal that the expression levels of PSAT1 were positively related to worse differentiation and vascular invasion of primary CRC lesions (Table 1).

PSAT1 promoted the malignant behaviors of CRC cells in vitro

We constructed PSAT1-overexpressed RKO and SW480 cell lines (Fig. 3A, B, Supplementary Fig. S1) and then conducted functional assays in vitro. According to the results of CCK-8 assay and clonogenic assay, overexpressing

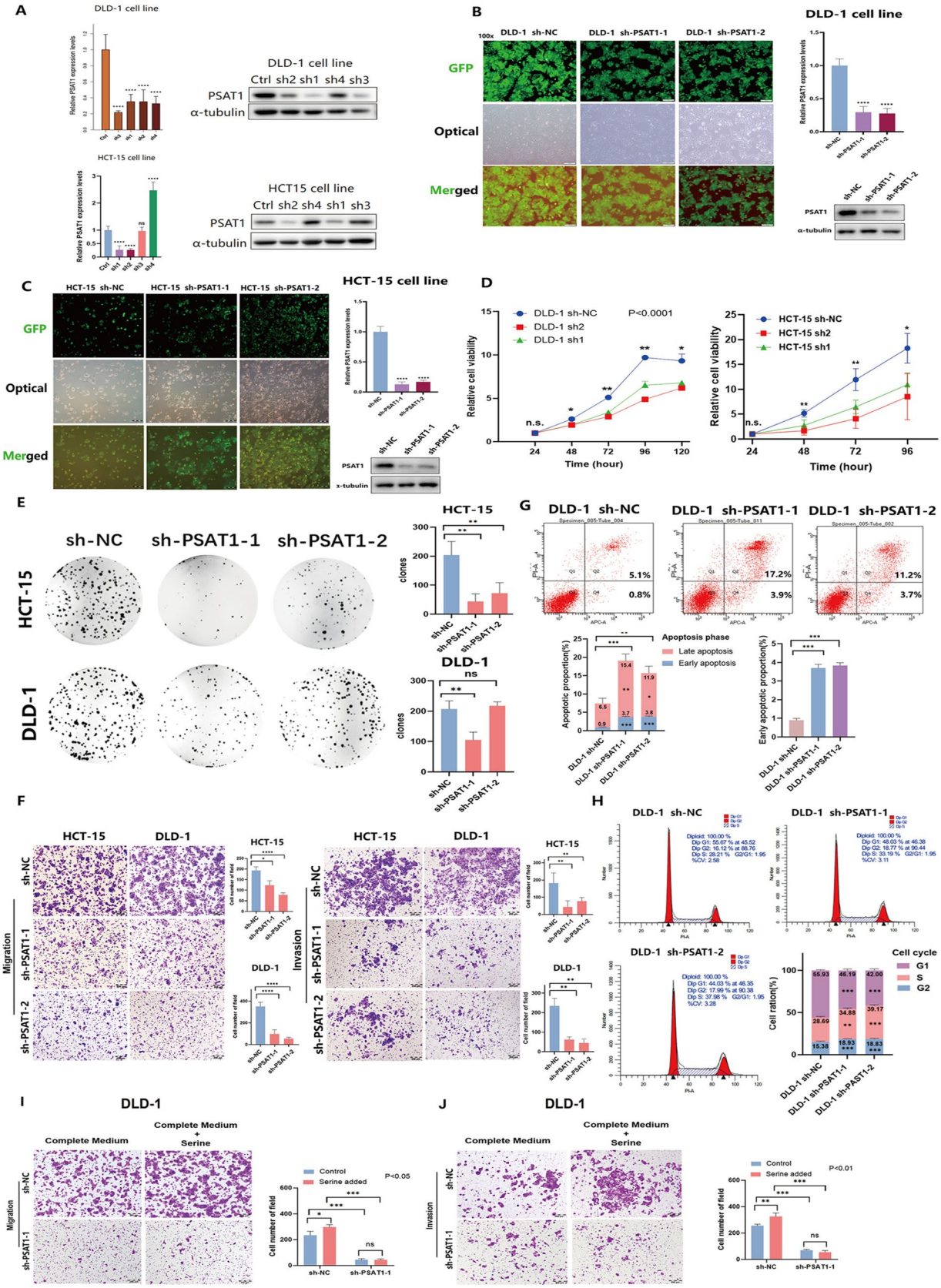
A
DLD-1 cell line
Relative PSAT1 expression levels
Ctrl sh2 sh1 sh4 sh3
PSAT1
α-tubulin
HCT-15 cell line
HCT15 cell line
Ctrl sh2 sh4 sh1 sh3
B
DLD-1 cell line
100×
DLD-1 sh-NC
DLD-1 sh-PSAT1-1
DLD-1 sh-PSAT1-2
GFP
Optical
Merged
C
HCT-15 cell line
HCT-15 sh-NC
HCT-15 sh-PSAT1-1
HCT-15 sh-PSAT1-2
x-tubulin
D
DLD-1 sh-NC
DLD-1 sh2
DLD-1 sh1
P<0.0001
Relative cell viability
Time (hour)
HCT-15 sh-NC
HCT-15 sh2
HCT-15 sh1
n.s.
E
sh-NC
sh-PSAT1-1
sh-PSAT1-2
HCT-15
DLD-1
clones
ns
G
DLD-1 sh-NC
DLD-1 sh-PSAT1-1
DLD-1 sh-PSAT1-2
5.1%
0.8%
17.2%
3.9%
11.2%
3.7%
Apoptosis phase
Late apoptosis
Early apoptosis
Apoptotic proportion(%)
Early apoptotic proportion(%)
F
Migration
Invasion
H
Diploid: 100.00 %
Dip G1: 55.67 % at 45.52
Dip G2: 15.12 % at 88.76
Dip S: 28.21 %
%CV: 2.58
Dip G1: 48.03 % at 46.38
Dip G2: 18.77 % at 90.44
Dip S: 33.19 %
%CV: 3.11
Dip G1: 44.03 % at 46.35
Dip G2: 17.99 % at 90.38
Dip S: 37.98 %
%CV: 3.28
Cell cycle
G1
S
G2
Cell ration(%)
I
J
Complete Medium
Complete Medium + Serine
Control
Serine added
P<0.05
P<0.01
Cell number of field

◂**Fig. 4** Loss-of-function assays of PAST1 in CRC cells in vitro. **A–C** Verification of the efficiency of stable knockdown of PSAT1 in DLD-1 (**A**, **B**) and HCT-15 (**A**, **C**) by WB and RT-qPCR assay, and the images including GFP fluorescence images, white light images, and merge images in DLD-1 and HCT-15 cells (on the left part of **B**, **C**). **D** CCK-8 assay, showing that stably knocking down PSAT1 inhibited the proliferation of DLD-1 and HCT-15 cells in vitro. **E** Clonogenic assay, showing that stably knocking down PSAT1 inhibited the colony formation of DLD-1 and HCT-15 cells. **F** Transwell migration assay and transwell invasion assay, showing that stably knocking down PSAT1 inhibited the migration and invasion of DLD-1 and HCT-15 cells. (**G**) Cell apoptosis detection by flow cytometry, showing that stably knocking down PSAT1 promoted the early and late apoptosis of DLD-1 cells, with early apoptosis being more significant. **H** Cell cycle detection by flow cytometry and bar chart, showing that stably knocking down PSAT1 affected the cell cycle and could induce arrest in the S and G2 phases of DLD-1 cells. **I, J** Transwell migration assay (**I**) and transwell invasion assay (**J**), showing the impact of adding exogenous serine to DLD-1 sh-NC and DLD-1 sh-PSAT1-1 on the migration and invasion abilities as compared with the impact of complete medium in vitro. The plots of the transwell migration assay are displayed on the left part and the bar chart is displayed on the right part. "ns" denotes no statistically significant difference; * indicates $p < 0.05$; ** signify $p < 0.01$; *** are used for $p < 0.001$; **** correspond to $p < 0.0001$

PSAT1 enhanced the proliferation of SW480 and RKO cells (Fig. 3C–E). The transwell migration assay showed that overexpressing PSAT1 enhanced the migration of SW480 and RKO cells ((Fig. 3F), and the cell cycle detection indicated that overexpressing PSAT1 induced an increase in the proportion of cells in the G1 phase, which implied that overexpressing PSAT1 could induce G1 arrest in SW480 cells (Fig. 3G).

After preliminary efficiency verification, we performed subsequent functional assays on the sh1 and sh2 groups of DLD-1 and HCT-15 (Fig. 4A–C). Our results showed that knocking down PSAT1 led to the suppression of the proliferation, migration, and invasion abilities of DLD-1 and HCT-15 cells in vitro (Fig. 4D-F). Knocking down PSAT1 led to a significant rise in the proportion of apoptotic DLD-1 cells. Among the increased apoptotic population, the percentage of late apoptotic cells exceeded that of early apoptotic cells. In addition, compared with late apoptotic cells, the fold increase of early apoptotic cells was more obvious after knocking down PSAT1 (Fig. 4G). The results of cell cycle detection indicated that the knockdown of PSAT1 was associated with an increased proportion of DLD-1 cells in the S and G2 phases, which implied that knocking down PSAT1 could induce S and G2 arrest in CRC (Fig. 4H).

To check whether the concentration of the serine affects the biological function of PSAT1, we supplemented sufficient exogenous serine (12 mm, effective concentration sourced from the literature [36]) in DLD-1 cells. The results showed that adding exogenous serine to the negative control (NC) group can partially rescue the migration and invasion abilities of CRC, but cannot rescue the inhibited invasion and migration abilities of the sh-PSAT1-1 group in vitro (Fig. 4I, J). The results suggested that PSAT1 might play an enzymatic-independent role in promoting CRC cells migration and invasion.

PSAT1 inhibited the Hippo tumor-suppressor pathway in CRC

To further explore how PSAT1 promotes CRC progression, we analyzed the biological pathways that PSAT1 was involved in by using the TCGA-COADREAD dataset. Analysis of the TCGA-COADREAD dataset showed that the expression level of PSAT1 was negatively correlated to the GSVA score of Hippo-related pathways, and the Hippo-related pathways were significantly enriched as the expression level of PSAT1 decreased in GSEA results (Fig. 5A, B). Then, we detected the expression of Hippo pathway-associated proteins in PSAT1 knockdown cell lines. In the DLD-1 cell line, inhibition of PSAT1 down-regulated the expression level of ID1, a known member of the oncogenic module of the Hippo pathway but no significant changes were witnessed at the overall expression levels of TAZ and YAP1 of the oncogenic modules (Fig. 5C). And no obvious trends were presented in YAP1 and phosphorylated YAP1, which suggested that the YAP1 protein was not dephosphorylated (Fig. 5C). In the SW480 cell line, overexpressing PSAT1 up-regulated the expression levels of oncogenic modules ID1, TAZ, and YAP1 in the Hippo pathway, but no significant changes were witnessed in phosphorylated YAP1 (Fig. 5D). Interestingly, further studies showed that in the DLD-1 cell line, TAZ and YAP1 transported into the nucleus were decreased after PSAT1 was knocked down (Fig. 5E).

AMOT was an important downstream molecule of PSAT1 in CRC

To further analyze the important downstream molecules of PSAT1 in CRC, we performed RNA-seq on DLD-1 sh-NC, sh-PSAT1-1, and sh-PSAT1-2. We analyzed and displayed the results in Volcano plots, Venn diagrams, Heat maps, and a Scatter plot (Fig. 6A–C, Supplementary Fig. S2A, B). We found that 335 DEGs were jointly up-regulated and 41 differentially expressed genes were jointly down-regulated upon PSAT1 knockdown.

We want to find through which downstream molecules PSAT1 may affect the Hippo pathway. AMOT can molecularly interact with YAP/TAZ [20], which is curated in the KEGG pathway diagram (Fig. 6D). Analyzing the CRC cell line RNA-seq data, we found that AMOT was among the up-regulated DEGs after PSAT1 was knocked down (Fig. 6E). We confirmed the correlation between PSAT1 and AMOT in DLD-1 and SW480 cells at the transcriptional level. Further RT-qPCR experiments confirmed that the expression

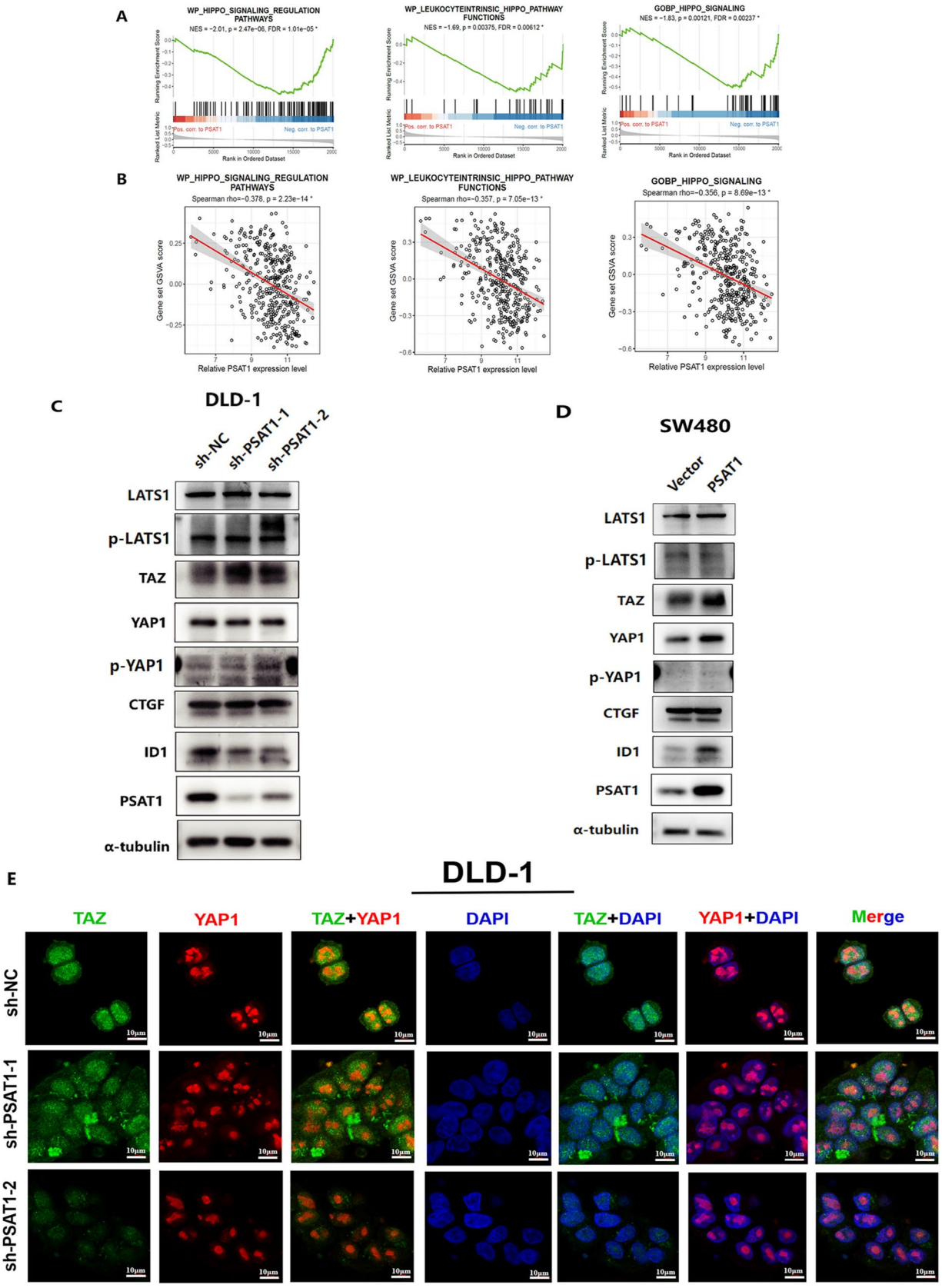
A
WP_HIPPO_SIGNALING_REGULATION PATHWAYS
NES = −2.01, p = 2.47e−06, FDR = 1.01e−05 *
WP_LEUKOCYTEINTRINSIC_HIPPO_PATHWAY FUNCTIONS
NES = −1.69, p = 0.00375, FDR = 0.00612 *
GOBP_HIPPO_SIGNALING
NES = −1.83, p = 0.00121, FDR = 0.00237 *
Running Enrichment Score
Ranked List Metric
Pos. corr. to PSAT1
Neg. corr. to PSAT1
Rank in Ordered Dataset
B
WP_HIPPO_SIGNALING_REGULATION PATHWAYS
Spearman rho=−0.378, p = 2.23e−14 *
WP_LEUKOCYTEINTRINSIC_HIPPO_PATHWAY FUNCTIONS
Spearman rho=−0.357, p = 7.05e−13 *
GOBP_HIPPO_SIGNALING
Spearman rho=−0.356, p = 8.69e−13 *
Gene set GSVA score
Relative PSAT1 expression level
C
DLD-1
sh-NC
sh-PSAT1-1
sh-PSAT1-2
LATS1
p-LATS1
TAZ
YAP1
p-YAP1
CTGF
ID1
PSAT1
α-tubulin
D
SW480
Vector
PSAT1
LATS1
p-LATS1
TAZ
YAP1
p-YAP1
CTGF
ID1
PSAT1
α-tubulin
E
DLD-1
TAZ
YAP1
TAZ+YAP1
DAPI
TAZ+DAPI
YAP1+DAPI
Merge
sh-NC
sh-PSAT1-1
sh-PSAT1-2
10μm

◂**Fig. 5** PSAT1 promoted CRC progression through the Hippo pathway. **A** GSEA enrichment plots, showing that down-regulation of PSAT1 expression level in CRC was significantly enriched in the Hippo pathway. The analysis was based on the TCGA-COADREAD dataset, where * denotes $p < 0.05$ and FDR < 0.25. **B** GSVA-Spearman correlation analysis plots, showing that a statistically significant negative correlation between the expression levels of PSAT1 and the signaling activity of the Hippo pathway. The analysis was based on the TCGA-COADREAD dataset, where * indicates $p < 0.05$. **C**, **D** WB results showed that PSAT1 activated oncogenic modules in the Hippo pathway at the protein level in PSAT1-inhibited DLD-1 cell line (**C**) and PSAT1-overexpressed SW480 cell line (**D**). To ensure that proteins of different molecular weights could be detected well, the samples derived from the same experiment or parallel experiments and that gels/blots were processed in parallel. All experimental samples and controls used for one comparative analysis were run on the same blot/gel. **E** Immunofluorescence analysis showing reduced nuclear localization of both TAZ and YAP in sh-PSAT1-1 and −2 groups, compared with the sh-NC group in DLD-1 (1260 × magnification)

of AMOT was negatively correlated with the expression of PSAT1 in DLD-1 and SW480 cells (Fig. 6F–I). These findings corroborated the data derived from the RNA-seq analysis we conducted on the DLD-1 cell line. We detected AMOT mRNA expression levels in the normal and CRC cell lines. Our results reveal that some cell lines have lower AMOT mRNA expression levels than the FHC and some have higher values than the FHC (Fig. 6J).

PSAT1 promoted the CRC progression by negatively regulating AMOT

AMOT encodes two protein isoforms: p80 and p130 [23]. In our RNA-seq data, we found that the expression levels of AMOT transcripts encoding p80 and p130, respectively, were jointly up-regulated in the sh-PSAT1 groups as compared with the sh-NC group (Fig. 7A). To validate the finding, we designed primers targeting the two transcripts in RT-qPCR separately. Consistently, the results showed that the expression of the p80 and p130 transcripts and the total AMOT were up-regulated in PSAT1 knockdown cells, compared with the sh-controls, and down-regulated in PSAT1-overexpressed cells, compared with the OV-controls (Fig. 7B–E, Supplementary Fig. S3A–C). However, when comparing the PSAT1-overexpression group with the OV-control group of RKO cells, no obvious changes were witnessed in the mRNA expression levels of total AMOT and AMOT transcripts p80 and p130 (Supplementary Fig. S3D). Furthermore, we measured the AMOT protein expression levels of DLD-1, SW480, and RKO cells through WB. Our results showed that AMOT expression was down-regulated in PSAT1-overexpressed cells, and up-regulated in PSAT1 knockdown cells (Fig. 7C, E, Supplementary Fig. S3E). The data suggested that PSAT1 negatively regulated AMOT in CRC cells. Therefore, our study reveals that up-regulation of PSAT1 expression can inhibit the expression of total AMOT and AMOT p80 and p130 isoforms, down-regulation of PSAT1 expression can promote the expression of total AMOT, AMOT p80, and AMOT p130 isoforms, and PSAT1 may play a critical role by simultaneously affecting the expression levels of the two AMOT isoforms.

Next, we sought to delineate the functional significance of AMOT in CRC. We knocked down AMOT in CRC cells (Supplementary Fig. S3F–K), and detected the impact of changed AMOT expression on the biological behavior of CRC cells in vitro. The CCK8 results suggested that the knockdown of AMOT slightly promoted the proliferation of DLD-1 cells and partially rescued the proliferation of DLD-1 cells impaired by PSAT1 knockdown (Fig. 7F). Consistently, knocking down AMOT partially rescued the in vitro colony formation ability of cancer cells impaired by PSAT1 knockdown in DLD-1 and HCT-15, but has little impact on the sh-NC groups of DLD-1 (Fig. 7G, H). The reason for the little impact may lie in the limited reaction time for siRNA and the low expression level of AMOT in the sh-NC groups.

To examine if AMOT affects the nuclear localization of YAP/TAZ, we performed immunofluorescence assays again. Our results revealed that DLD-1 cells transfected with sh-PSAT1-1 + siNC exhibited a significant reduction in the nuclear localization of YAP and TAZ compared to those treated with sh-NC + siNC, which is consistent with our observed results (Fig. 5E). Conversely, silencing AMOT in sh-NC cells led to an increased nuclear localization of these two proteins. Moreover, AMOT silencing partially restored the diminished nuclear localization of YAP and TAZ observed in sh-PSAT1-transfected cells (Fig. 7I). This suggested that AMOT participates in the regulatory mechanism by which PSAT1 knockdown diminishes the nuclear translocation of TAZ and YAP. Hence, we concluded that PSAT1 could suppress AMOT expression, facilitating the localization of YAP/TAZ from the cytoplasm into the nucleus, therefore boosting CRC progression.

After going through the literature, we learned that AMOT participated in regulating cell migration of endothelial cells and vascularization [23]. We wondered whether the up-regulation of AMOT caused by knocking down PSAT1 in CRC was sufficient to make a difference in blood vessel-related pathways. By further analyzing our DLD-1 cell line through RNA-seq, we found that the gene sets for “blood vessel development" and "cell surface interaction on the blood vessel wall" were significantly enriched in the PSAT1 knockdown groups (Supplementary Fig. S4A-B). Of note, AMOT was among the top common core enrichment genes in the gene set for "blood vessel development" (Supplementary Fig. S4A-B). Considering that AMOT is reported to be mainly expressed in blood vessels, we used TISCH2 (http://tisch.comp-genomics.org/home/) to conduct single-cell

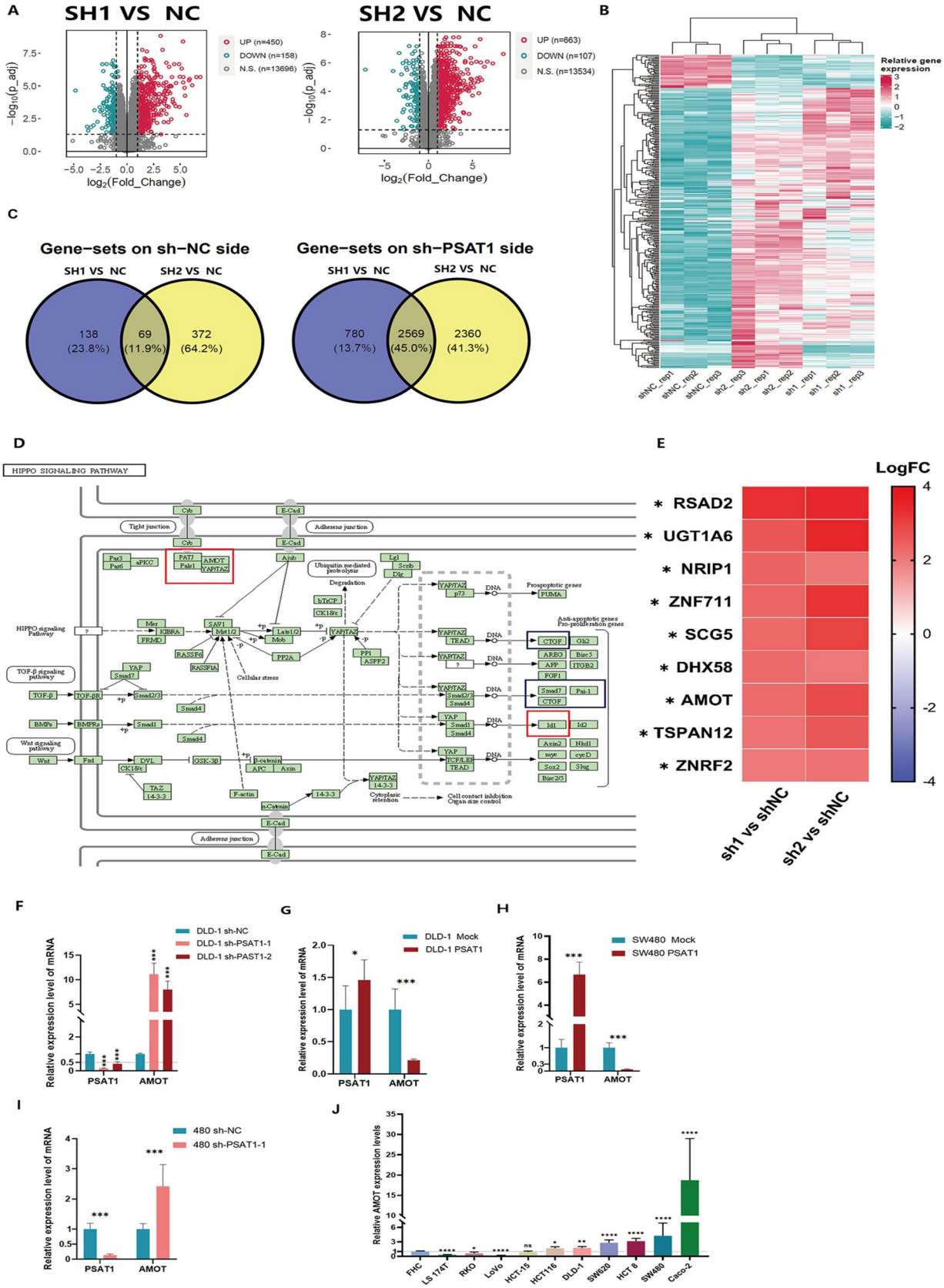
A
SH1 VS NC
UP (n=450)
DOWN (n=158)
N.S. (n=13696)
−log10(p_adj)
log2(Fold_Change)
SH2 VS NC
UP (n=663)
DOWN (n=107)
N.S. (n=13534)
B
Relative gene expression
shNC_rep1
shNC_rep2
shNC_rep3
sh2_rep3
sh2_rep1
sh2_rep2
sh1_rep1
sh1_rep2
sh1_rep3
C
Gene−sets on sh−NC side
SH1 VS NC
SH2 VS NC
138 (23.8%)
69 (11.9%)
372 (64.2%)
Gene−sets on sh−PSAT1 side
780 (13.7%)
2569 (45.0%)
2360 (41.3%)
D
HIPPO SIGNALING PATHWAY
E
LogFC
* RSAD2
* UGT1A6
* NRIP1
* ZNF711
* SCG5
* DHX58
* AMOT
* TSPAN12
* ZNRF2
sh1 vs shNC
sh2 vs shNC
F
DLD-1 sh-NC
DLD-1 sh-PSAT1-1
DLD-1 sh-PAST1-2
Relative expression level of mRNA
PSAT1
AMOT
G
DLD-1 Mock
DLD-1 PSAT1
H
SW480 Mock
SW480 PSAT1
I
480 sh-NC
480 sh-PSAT1-1
J
Relative AMOT expression levels
FHC
LS 174T
RKO
LoVo
HCT-15
HCT116
DLD-1
SW620
HCT 8
SW480
Caco-2

◂**Fig. 6** Core downstream molecule selection based on RNA-seq of PSAT1 knockdown CRC cells. **A** Volcano plots showing the expression levels of DEGs between two sh-PSAT1 groups (sh1, sh2) and the sh-NC of DLD-1 cells in our cell line RNA-seq. Green and red data points were filtered according to |limma-voom logFC|> 1 and p adjust < 0.05. **B** Heat map showing the normalized values of $\log_2$ FPKM, that is, the relative gene expression levels of three biological replicate samples of DLD-1 sh-NC, sh-PSAT1-1, and sh-PSAT1-2 in our cell line RNA-seq. **C** Venn diagram showing the up-regulated and down-regulated enriched gene sets and overlapping gene sets found in GSEA. The sh-PSAT1 groups and the NC group meet $p < 0.05$ and FDR < 0.25; common up-regulated gene sets meet NES_sh1 vs NC > 0 and NES_sh2 vs NC > 0; and common down-regulated gene sets meet NES_sh1 vs NC < 0 and NES_sh2 vs NC < 0. **D** Schematic diagram of the relationship between the AMOT protein and the Hippo signaling pathway, based on KEGG. **E** Heat map showing the filtering results obtained when DEGs generated in RNA-seq after PSAT1 in the DLD-1 cell line was stably knocked down were filtered according to limma-voom logFC > 2 and adj $p < 0.05$ and FPKM were filtered according to sh-NC > 0.5, sh1 > 1, and sh2 > 1. The results showed that AMOT was ranked seventh among the obtained nine genes. **F–I** RT-qPCR results showed the PSAT1 and AMOT expression levels. The tested cells include the control (sh-NC, Mock) groups, PSAT1-overexpression groups, sh-PSAT1 groups based on DLD-1 and SW480 cells, respectively. **J** RT-qPCR results showed a correlation between PSAT1 and AMOT expression levels. "ns" denotes no statistically significant difference; * indicates $p < 0.05$; ** signify $p < 0.01$; *** are used for $p < 0.001$; **** correspond to $p < 0.0001$

RNA-seq analysis of the CRC-EMTAB8107 and CRC-GSE166555 databases. As indicated in the results, in CRC, AMOT is expressed not only within vascular endothelial cells and immune cells but also within benign and malignant colorectal epithelial cells (Supplementary Fig. S4C-D). The detected transcription and translation levels of AMOT in our cell lines also support this finding. In a word, PSAT1 may play a crosstalk role between CRC cells and the tumor microenvironment by mediating a vascular-related molecule AMOT, thereby affecting the progression of CRC.

PSAT1 promoted CRC progression in vivo

The results showed that in the sh-PSAT1 group, the tumor growth was slower, the tumor weight was significantly reduced, and tumors were not formed in most nude mice compared with the sh-NC group. These findings suggested that PSAT1 confers its oncogenic properties through the facilitation of cellular proliferation in vivo. (Fig. 8A–D). The HE and IHC results of the subcutaneous tumors showed that after PSAT1 was knocked down, the Ki-67 proliferation index was simultaneously down-regulated and AMOT was up-regulated (Fig. 8E). In addition, the IHC results of paraffin sections of human CRC tissue also proved the negative correlation between PSAT1 and AMOT (Fig. 8F).

Discussion

CRC ranks among the top three malignant tumors with the highest morbidity and mortality worldwide [1]. Although early screening and related treatments are becoming more efficacious, advanced CRC benefits are very limited and the probability of postoperative recurrence and metastasis is still high [2]. Therefore, seeking efficacious tumor biomarkers and exploring their potential roles in the progression and metastasis of CRC are of profound significance for clarifying the pathogenesis, long-term treatment, and early screening of CRC.

PSAT1 is selected as the tumor biomarker based on the CRC databases. PSAT1 is a pivotal catalyst within de novo SSP [3]. Some studies report that PSAT1 expression is up-regulated in various types of tumors such as hepatocellular carcinoma, lung carcinoma, cervical carcinoma, and ovarian carcinoma, promoting tumor progression [9, 15–17, 37]. Some studies report that PSAT1 inhibits tumor progression, mainly focusing on the central nervous system [38, 39]. Such findings suggest that PSAT1 may play disparate roles in diverse types of cancers. Our bioinformatics analysis showed that the expression of PSAT1 was up-regulated at the colorectal adenoma stage and continued to be up-regulated as the disease progressed. Our findings indicated that PSAT1 demonstrates elevated expression levels across a spectrum of CRC cell lines as well as in clinical samples of CRC tissue. Furthermore, our evidence revealed a positive correlation between elevated expression levels of PSAT1 and adverse histological features in CRC about poor differentiation and increased vascular invasion. PSAT1 remained up-regulated in LN metastases and liver metastases. In addition, public website analysis revealed that PSAT1 could be detected in plasma, which may be applied in early screening. These findings indicated that PSAT1 may be involved throughout the occurrence, development, and metastasis of CRC. Our in vitro functional assays also verified that PSAT1 enhanced CRC proliferation, migration, and invasion, inhibited CRC apoptosis, and affected the cell cycle. Our in vivo assays verified that PSAT1 promoted CRC progression.

Existing studies on PSAT1 in CRC cover drug resistance [10, 12, 40], serine synthesis [11, 36], cell cycle progression [11], and methylation [11]. And fewer studies on PSAT1 focus on its molecular mechanisms in CRC [10–12]. For example, the overexpressed PSAT1 is known to play a significant carcinogenesis role in CRC, which is also reported in breast carcinoma and lung carcinoma, because it increases cyclin D1 expression by promoting mTOR phosphorylation and degrades cyclin D1 by inhibiting the GSK3β enzyme during cell cycle progression [9, 11, 41]. And Montrose et al. found that in CRC both exogenous serine and endogenous serine synthesis driven by highly expressed PSAT1

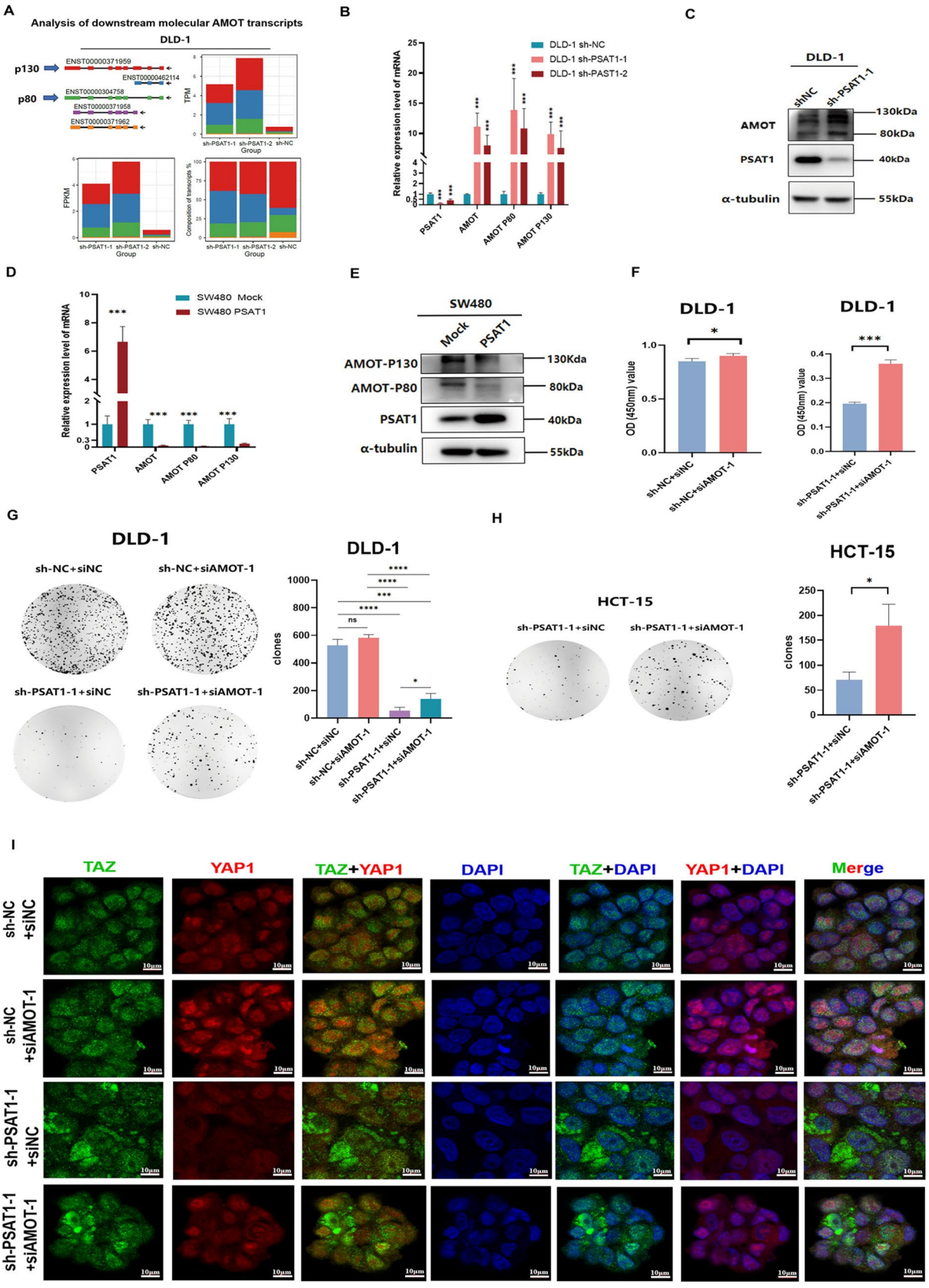
A
Analysis of downstream molecular AMOT transcripts
DLD-1
p130
p80
ENST00000371959
ENST00000462114
ENST00000304758
ENST00000371958
ENST00000371962
TPM
FPKM
Composition of transcripts %
sh-PSAT1-1 sh-PSAT1-2 sh-NC
Group
B
DLD-1 sh-NC
DLD-1 sh-PSAT1-1
DLD-1 sh-PAST1-2
Relative expression level of mRNA
PSAT1
AMOT
AMOT P80
AMOT P130
C
DLD-1
shNC
sh-PSAT1-1
AMOT
PSAT1
α-tubulin
130kDa
80kDa
40kDa
55kDa
D
SW480 Mock
SW480 PSAT1
Relative expression level of mRNA
E
SW480
Mock
PSAT1
AMOT-P130
AMOT-P80
PSAT1
α-tubulin
130Kda
80kDa
40kDa
55kDa
F
DLD-1
OD (450nm) value
sh-NC+siNC
sh-NC+siAMOT-1
DLD-1
OD (450nm) value
sh-PSAT1-1+siNC
sh-PSAT1-1+siAMOT-1
G
DLD-1
sh-NC+siNC
sh-NC+siAMOT-1
sh-PSAT1-1+siNC
sh-PSAT1-1+siAMOT-1
DLD-1
clones
sh-NC+siNC
sh-NC+siAMOT-1
sh-PSAT1-1+siNC
sh-PSAT1-1+siAMOT-1
H
HCT-15
sh-PSAT1-1+siNC
sh-PSAT1-1+siAMOT-1
HCT-15
clones
sh-PSAT1-1+siNC
sh-PSAT1-1+siAMOT-1
I
TAZ
YAP1
TAZ+YAP1
DAPI
TAZ+DAPI
YAP1+DAPI
Merge
sh-NC +siNC
sh-NC +siAMOT-1
sh-PSAT1-1 +siNC
sh-PSAT1-1 +siAMOT-1
10μm

◂**Fig. 7** PSAT1 promoted CRC cells proliferation via negatively regulating AMOT. **A** Bar chart, the analysis data sourced from FPKM obtained through RNA-seq of the DLD-1 cell line after PSAT1 was stably knocked down. **B–E** RT-qPCR and WB results showed the correlation between the expression of PSAT1, AMOT, AMOT p80, and AMOT p130. The cells including the stable knockdown PSAT1 groups from DLD-1 and the stable overexpression PSAT1 groups from SW480. **F** CCK-8 assay, showing the cell proliferation ability after AMOT was transiently knocked down for 36 h in DLD-1 cells by detecting the (optical density) OD values after 3 days. The cells used for transiently knocking down AMOT were the sh-NC group and the sh-PAST1-1 group of DLD-1. **G, H** Clonogenic assay results (left) and bar charts (right). The cells used to transiently knockdown AMOT were the sh-NC group and the sh-PAST1-1 group of DLD-1 (**G**) and the sh-PAST1-1 group of HCT-15 (**H**). **I** Immunofluorescence assay of TAZ and YAP in sh-NC or sh-PSAT1-1 DLD-1 cells which were further transfected with siNC or siAMOT-1. The results indicated that AMOT potentially plays a role in the PSAT1-mediated enhancement of TAZ and YAP's nuclear accumulation (1260 × magnification). "ns" denotes no statistically significant difference; * indicates $p < 0.05$; ** signify $p < 0.01$; *** are used for $p < 0.001$; **** correspond to $p < 0.0001$

enhanced the proliferation of colon cancer and the resistance to 5-FU [10].

The phenomenon of interference with PSAT1 in exogenous serine existence blocks tumor progression [43] implying that PSAT1 may have a carcinogenic effect different from its serine biosynthesis-associated role [15]. Therefore, it is highly likely that PSAT1 exerts other important carcinogenic functions in addition to its metabolic effects. However, the non-metabolic role of PSAT1, for instance, lung carcinoma, breast carcinoma, and hepatocellular carcinoma, is only mentioned in a few reports [15, 17, 18]. For example, a study on lung adenocarcinoma suggested that the non-enzymatic function of PSAT1 contributed to cancer development by inhibiting the IRF1-IFN-γ axis [18]. Jiang et al. reported that PSAT1 promoted metastasis of tumors by playing a similar role as the p53-72Pro variant [15]. In addition, some reports believe that PSAT1 is involved in different phases of the same tumor due to its metabolic and non-metabolic activities. For example, abnormal up-regulation of PSAT1 leads to resistance to erlotinib and metastasis in lung cancer [16]. Certainly, some studies did not further explore whether the SSP played a role in the tumor processes [42, 44]. Zhu et al. confirmed that PSAT1 promoted distant metastasis in ER-negative breast carcinoma by activating the Notch and β-catenin pathways [42]. Biyik-Sit et al. confirmed that nuclear PKM2 contributed to PSAT1-mediated EGFR-activated lung cancer cell migration by interacting with PSAT1 [44].

Here, we conducted in vitro functional assays and found that the addition of exogenous serine cannot completely restore the invasion or migration ability of CRC cells in vitro, and this implied that PSAT1 might play an unknown role in CRC regardless of its participation in SSP. Besides, we gained more insights into the PSAT1 role in CRC progression and elucidated its underlying mechanisms. Our evidence showed that PSAT1 is closely related to the Hippo pathway. Inhibition of PSAT1 down-regulated the expression level of ID1, a known member of the oncogenic module of the Hippo pathway. For the past few years, the Hippo pathway has attracted much attention in cancer research [19].

Moreover, our evidence showed that knocking down PSAT1 in CRC did not change the overall expression of TAZ/YAP proteins, but decreased the translocation of TAZ/YAP into the nucleus. This function of PSAT1 is independent of its known metabolic function. It suggested that after PSAT1 was knocked down, the YAP/TAZ might be isolated or its degradation might be accelerated in the cytoplasm by a factor, thereby decreasing the translocation of YAP/TAZ into the nucleus, and finally inhibiting tumor growth. YAP/TAZ, which acted as an oncogenic module in the Hippo pathway [19], is also regulated in other ways [22], but the molecular mechanism remains not fully clear.

AMOT molecularly interacts with YAP/TAZ, which is one of its most important known functions [20]. Our RNA-seq in cell lines further revealed that the knockdown of PSAT1 up-regulated AMOT, a member of angiostatin-binding proteins [23]. Research on various malignant tumors, for instance, DLBCL, lung carcinoma, and gastric carcinoma, suggested that AMOT and its isoforms serve as tumor suppressors [25–31]. However, studies on other malignant tumors such as CRC, renal cell cancer, and breast carcinoma suggested that AMOT and its isoforms serve as tumor promoters [23, 32–35]. However, the upstream regulator of AMOT remains largely unclear. Furthermore, the relationship between PSAT1 and AMOT has not been found yet. We found that PSAT1 was negatively correlated with AMOT by reducing the expression of both of the two isoforms of AMOT at a cellular level. In addition, the IHC study using clinical samples also confirmed that the expression of PSAT1 was negatively correlated with the expression of AMOT at the tissue level. Furthermore, our evidence demonstrated that knocking down AMOT could partially rescue the inhibitory phenotype of PSAT1 in the malignant proliferation of CRC cells in vitro. Therefore, we concluded that PSAT1 could inhibit AMOT in CRC and AMOT is involved in the tumor-promoting effect of PSAT1. However, more experimental studies are needed to investigate how PSAT1 exerts its oncogenic effects through AMOT. For example, transgenic animal models can provide valuable in vivo evidence for the effect of PSAT1 on the biological behavior of tumors by regulating AMOT.IHC analysis with more clinical samples and multiple-factor survival analysis can further confirm PSAT1 regulation of AMOT and its effect on prognosis.

It is known that AMOT regulates YAP and TAZ proteins in the Hippo pathway, but there is controversy on the direction of action and the mechanism of AMOT on YAP/TAZ

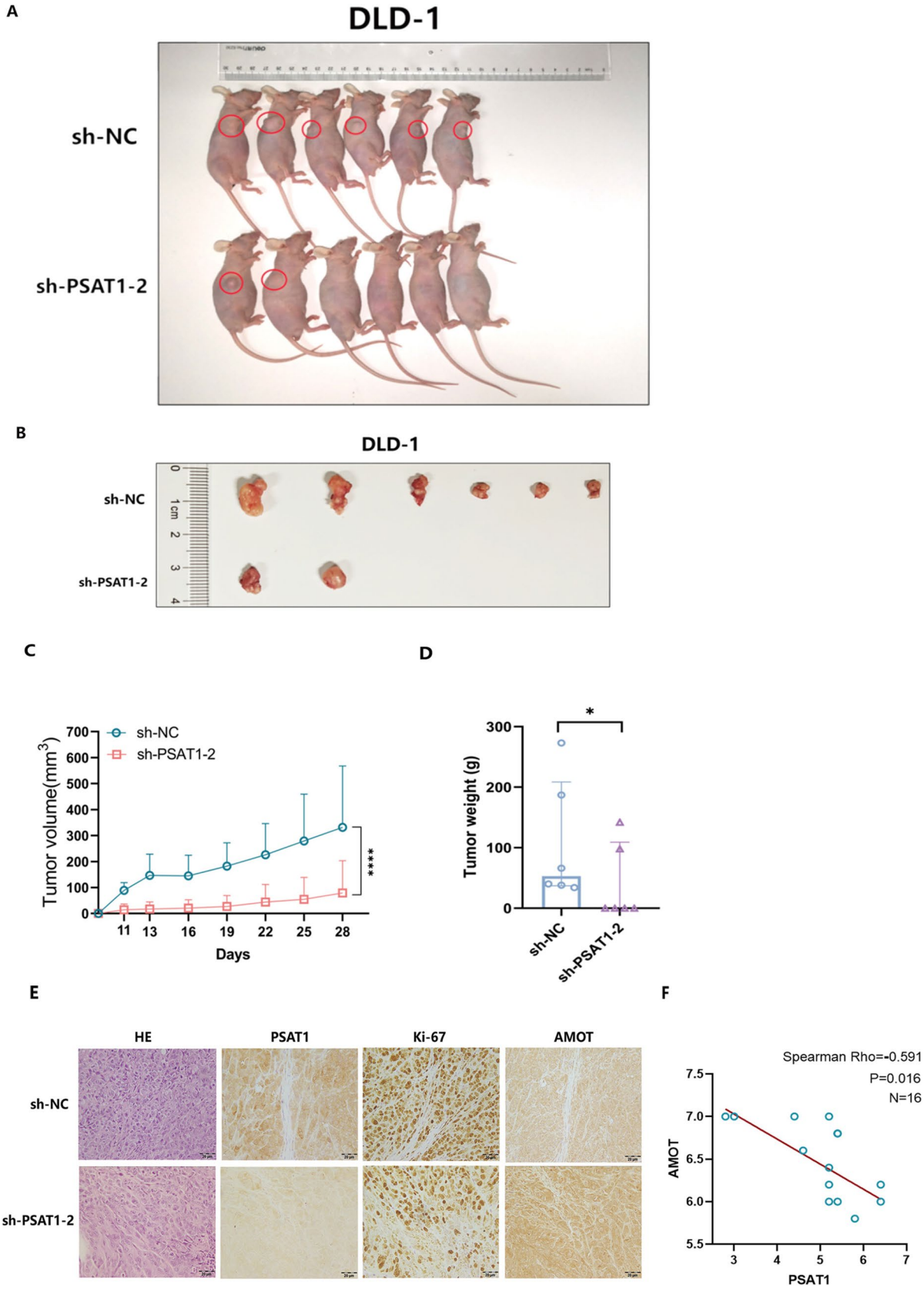
A
DLD-1
sh-NC
sh-PSAT1-2
B
DLD-1
sh-NC
sh-PSAT1-2
1cm
C
sh-NC
sh-PSAT1-2
Tumor volume(mm3)
Days
****
D
Tumor weight (g)
*
sh-NC
sh-PSAT1-2
E
HE
PSAT1
Ki-67
AMOT
sh-NC
sh-PSAT1-2
F
Spearman Rho=-0.591
P=0.016
N=16
AMOT
PSAT1

◂**Fig. 8** PSAT1 promoted CRC cell proliferation in vivo. **A** Image of tumor-bearing nude mice. **B** Representative image of xenograft tumors in BALB/c-nu mice injected with the indicated cells. **C** Tumor growth curve of tumor-bearing nude mice. **D** Xenograft tumor weight graph. **E** IHC expression of PSAT1, AMOT, and Ki-67 in the same HE tumor area. **F** Correlation analysis based on the IHC scores of PSAT1 and AMOT in serial paraffin sections of tissue of 16 CRC cases

[25, 33]. Zhang et al. confirmed that AMOT dephosphorylates YAP and promotes YAP entering the nucleus from the cytoplasm to activate the YAP-ERK and PI3K-AKT pathways, which enhanced the malignant potential in CRC [33]. Nevertheless, in our study, PSAT1 knockdown up-regulated AMOT but did not affect the phosphorylation level of YAP. Another research on lung cancer suggested that AMOT sequestered YAP /TAZ in the cytoplasm to reduce the transport of YAP/TAZ into the nucleus and knocking down YAP/TAZ prevented the malignant potential of cancer cells that might be due to the lack of AMOT [25]. This is consistent with our immunofluorescence results that knocking down AMOT partially rescued the reduced nuclear localization of YAP/TAZ caused by PSAT1 knockdown in CRC. This observation points to a role for AMOT in the regulatory pathway affected by PSAT1 knockdown, most likely modulating the nuclear translocation of these key transcriptional coactivators. While our results are suggestive of this mechanism strongly, we acknowledge that additional experiments are necessary to rigorously substantiate our conclusions. For example, nuclear-cytoplasmic separation experiments on YAP/TAZ, the in vivo rescue experiment, and the detection of AMOT phosphorylation can further confirm our conclusions and make the mechanism more complete. In addition, the specific mechanism by which PSAT1 affects the expression of AMOT needs to be further studied, such as what transcription factors may mediate the suppressive effect of PSAT1 on the expression of AMOT, or whether PSAT1 affects the expression of AMOT through a serine-dependent pathway mechanism.

In addition, we returned to the first major function of AMOT. AMOT may negatively mediate the effects of angiostatin and be related to the migration of endothelial cells during vascularization and may be related to cell-to-cell junctions in endothelial cells [23, 45–47]. A few research also reported the mechanism of how AMOT acted as a vascular-related molecule to affect vascular endothelial cells [48]. The relationship between Hippo-YAP/TAZ signaling and angiogenesis has also been discussed [49]. However, how AMOT regulating or crosstalking between normal blood vessels and tumor blood vessels to affect tumor progression remains largely unknown. In addition, no literature elaborates on the connection between PSAT1 and vasculature-related molecules. In our study, our cell line RNA-seq results confirmed that vasculature-related pathways, where AMOT resides, were significantly enriched after PSAT1 was knocked down. This finding suggested that after being negatively induced by PSAT1, AMOT may serve its first major role in affecting the tumor microenvironment and promoting CRC metastasis. Our IHC results also indicated that PSAT1 is closely related to vascular invasion. No mechanisms of PSAT1 in the tumor microenvironment have been reported yet. That is why deeper research on this part will bring a new perspective to reveal the role of PSAT1 in the interaction between tumors and the tumor microenvironment, and provide an experimental basis for the application of PSAT1 in anti-tumor.

In summary, our study indicated that PSAT1 plays a new non-metabolic role in promoting the progression of CRC by negatively regulating AMOT and inhibiting the Hippo pathway. Hence, PSAT1 might become a potential therapeutic target for CRC.

Supplementary Information The online version contains supplementary material available at https://doi.org/10.1007/s11010-024-05194-8.

Acknowledgements The authors are grateful for the technical support of Guanglong Liu.

Author contributions Jie Lin directed the project, obtained funding, provided resources, and supervision of the study. Jie Lin and Minshan Tang designed the study. Minshan Tang performed the most part of the experiments, analyzed data, generated the bulk of the experimental results, and wrote the manuscript. Minshan Tang and Kai Song visualized and interpreted the data. Kai Song performed bioinformatic analyses, assisted in the completion of the experiments, and polished the manuscript. Danning Xie, Xinyu Yuan, Yaxuan Wang, Zhiyang Li, and Xiaotong Zhu participated in the experiments and contributed to the research data. Kai Song, Minshan Tang, Xiansheng Lu, and Jie Lin revised the article. Xiansheng Lu and Le Xiong assisted in interpreted the data. Liang Guo and Wenqian Zhou contributed to the collection of clinical samples. All authors have read and agreed to the published version of the manuscript.

Funding This work was supported by grants from National Natural Science Foundation of China (Grant No. 82173298).

Data availability The datasets supporting the conclusions of this article are available in the [GEO] repository, [200041657, 200074602 and hyperlink to datasets in https://www.ncbi.nlm.nih.gov/geo/]; in the [UCSC Xena] repository, [TCGA-COADREAD and hyperlink to dataset in https://xenabrowser.net/datapages/]. The cell line RNA-seq results supporting the conclusions of this article are included within the article and its additional files. Materials, additional data, and the raw data supporting the conclusions of this article will be made available by the authors on request.

Declarations

Conflict of interest The authors declare no conflicts of interest.

Ethical approval The study was conducted in accordance with the Declaration of Helsinki. This work was approved by the Medical Ethics Committee of Nanfang Hospital, Southern Medical University, China (approval number: NFEC-2024–334).

Informed consent Informed consent was obtained from all subjects involved in the study.

Consent to participate The animal study protocol was approved by the Institutional Animal Care and Use Committee (IACUC) and Southern Medical University Experimental Animal Ethics Committee in Guangzhou, China (approval number: SMUL2023081).

Consent for publication All the authors agree to publish this paper.

References

1. Sung H, Ferlay J, Siegel RL, Laversanne M, Soerjomataram I, Jemal A, Bray F (2021) Global Cancer Statistics 2020: GLOBOCAN Estimates of Incidence and Mortality Worldwide for 36 Cancers in 185 Countries. CA Cancer J Clin 71(3):209–49. https://doi.org/10.3322/caac.21660
2. Siegel RL, Miller KD, Fuchs HE, Jemal A (2021) Cancer Statistics, 2021. CA Cancer J Clin 71(1):7–33. https://doi.org/10.3322/caac.21654
3. Geeraerts SL, Heylen E, de Keersmaecker K, Kampen KR (2021) The ins and outs of serine and glycine metabolism in cancer. Nat Metab 3(2):131–41. https://doi.org/10.1038/s42255-020-00329-9
4. Faubert B, Solmonson A, Deberardinis RJ (2020) Metabolic reprogramming and cancer progression. Science 368(6487):5473. https://doi.org/10.1126/science.aaw5473
5. Xia L, Oyang L, Lin J, Tan S, Han Y, Wu N, Yi P, Tang L, Pan Q, Rao S, Liang J, Tang Y, Su M, Luo X, Yang Y, Shi Y, Wang H, Zhou Y, Liao Q (2021) The cancer metabolic reprogramming and immune response. Mol Cancer 20(1):28. https://doi.org/10.1186/s12943-021-01316-8
6. Nenkov M, Ma Y, Gaßler N, Chen Y (2021) Metabolic reprogramming of colorectal cancer cells and the microenvironment: implication for therapy. Int J Mol Sci. 22(12):6262. https://doi.org/10.3390/ijms22126262
7. Yang X,Li C,Chen Y. Phosphoserine Aminotransferase 1: A Metabolic Enzyme Target of Cancers. *Curr Cancer Drug Targets*. 2023; **23**(3): 171–86.https://doi.org/10.2174/1568009622666220829105300
8. Li AM, Ye J (2020) Reprogramming of serine, glycine and one-carbon metabolism in cancer. Biochim Biophys Acta Mol Basis Dis 1866(10):165841. https://doi.org/10.1016/j.bbadis.2020.165841
9. Gao S, Ge A, Xu S, You Z, Ning S, Zhao Y, Pang D (2017) PSAT1 is regulated by ATF4 and enhances cell proliferation via the GSK3β/β-catenin/cyclin D1 signaling pathway in ER-negative breast cancer. J Exp Clin Cancer Res. 36(1):179. https://doi.org/10.1186/s13046-017-0648-4
10. Montrose DC, Saha S, Foronda M, Mcnally EM, Chen J, Zhou XK, Ha T, Krumsiek J, Buyukozkan M, Verma A, Elemento O, Yantiss RK, Chen Q, Gross SS, Galluzzi L, Dow LE, Dannenberg AJ (2021) Exogenous and endogenous sources of serine contribute to colon cancer metabolism, growth, and resistance to 5-fluorouracil. Cancer Res 81(9):2275–88. https://doi.org/10.1158/0008-5472.Can-20-1541
11. Wang H, Cui L, Li D, Fan M, Liu Z, Liu C, Pan S, Zhang L, Zhang H, Zhao Y (2020) Overexpression of PSAT1 regulated by G9A sustains cell proliferation in colorectal cancer. Signal Transduct Target Ther 5(1):47. https://doi.org/10.1038/s41392-020-0147-5
12. Vié N, Copois V, Bascoul-Mollevi C, Denis V, Bec N, Robert B, Fraslon C, Conseiller E, Molina F, Larroque C, Martineau P, Del Rio M, Gongora C (2008) Overexpression of phosphoserine aminotransferase PSAT1 stimulates cell growth and increases chemoresistance of colon cancer cells. Mol Cancer 7:14. https://doi.org/10.1186/1476-4598-7-14
13. Wang M, Yue S, Yang Z (2023) Downregulation of PSAT1 inhibits cell proliferation and migration in uterine corpus endometrial carcinoma. Sci Rep 13(1):4081. https://doi.org/10.1038/s41598-023-31325-0
14. Ye J, Huang X, Tian S, Wang J, Wang H, Feng H, Zhao X, Cao S, Xuan Y, Li X, Ma X, Huang Y, Zhang X (2024) Upregulation of serine metabolism enzyme PSAT1 predicts poor prognosis and promotes proliferation, metastasis and drug resistance of clear cell renal cell carcinoma. Exp Cell Res. 437(1):113977. https://doi.org/10.1016/j.yexcr.2024.113977
15. Jiang J, Chen HN, Jin P, Zhou L, Peng L, Huang Z, Qin S, Li B, Ming H, Luo M, Xie N, Gao W, Nice EC, Yu Q, Huang C (2023) Targeting PSAT1 to mitigate metastasis in tumors with p53–72Pro variant. Signal Transduct Target Ther 8(1):65. https://doi.org/10.1038/s41392-022-01266-7
16. Luo MY, Zhou Y, Gu WM, Wang C, Shen NX, Dong JK, Lei HM, Tang YB, Liang Q, Zou JH, Xu L, Ma P, Zhuang G, Bi L, Xu L, Zhu L, Chen HZ, Shen Y (2022) Metabolic and nonmetabolic functions of PSAT1 coordinate signaling cascades to confer EGFR inhibitor resistance and drive progression in lung adenocarcinoma. Cancer Res 82(19):3516–31. https://doi.org/10.1158/0008-5472.Can-21-4074
17. Metcalf S, Dougherty S, Kruer T, Hasan N, Biyik-Sit R, Reynolds L, Clem BF (2020) Selective loss of phosphoserine aminotransferase 1 (PSAT1) suppresses migration, invasion, and experimental metastasis in triple negative breast cancer. Clin Exp Meta 37(1):187–97. https://doi.org/10.1007/s10585-019-10000-7
18. Chan YC, Chang YC, Chuang HH, Yang YC, Lin YF, Huang MS, Hsiao M, Yang CJ, Hua KT (2020) Overexpression of PSAT1 promotes metastasis of lung adenocarcinoma by suppressing the IRF1-IFNγ axis. Oncogene 39(12):2509–22. https://doi.org/10.1038/s41388-020-1160-4
19. Cunningham R, Hansen CG (2022) The Hippo pathway in cancer: YAP/TAZ and TEAD as therapeutic targets in cancer. Clin Sci (Lond) 136(3):197–222. https://doi.org/10.1042/cs20201474
20. Chan SW, Lim CJ, Chong YF, Pobbati AV, Huang C, Hong W (2011) Hippo pathway-independent restriction of TAZ and YAP by angiomotin. J Biol Chem 286(9):7018–26. https://doi.org/10.1074/jbc.C110.212621
21. Lei QY, Zhang H, Zhao B, Zha ZY, Bai F, Pei XH, Zhao S, Xiong Y, Guan KL (2008) TAZ promotes cell proliferation and epithelial-mesenchymal transition and is inhibited by the hippo pathway. Mol Cell Biol 28(7):2426–36. https://doi.org/10.1128/mcb.01874-07
22. Piccolo S, Panciera T, Contessotto P, Cordenonsi M (2023) YAP/TAZ as master regulators in cancer: modulation, function and

therapeutic approaches. Nat Cancer 4(1):9–26. https://doi.org/10.1038/s43018-022-00473-z
23. Lv M, Shen Y, Yang J, Li S, Wang B, Chen Z, Li P, Liu P, Yang J (2017) Angiomotin family members: oncogenes or tumor suppressors? Int J Biol Sci 13(6):772–81. https://doi.org/10.7150/ijbs.19603
24. Ernkvist M, Birot O, Sinha I, Veitonmaki N, Nyström S, Aase K, Holmgren L (2008) Differential roles of p80- and p130-angiomotin in the switch between migration and stabilization of endothelial cells. Biochim Biophys Acta 1783(3):429–37. https://doi.org/10.1016/j.bbamcr.2007.11.018
25. Hsu YL, Hung JY, Chou SH, Huang MS, Tsai MJ, Lin YS, Chiang SY, Ho YW, Wu CY, Kuo PL (2015) Angiomotin decreases lung cancer progression by sequestering oncogenic YAP/TAZ and decreasing Cyr61 expression. Oncogene 34(31):4056–68. https://doi.org/10.1038/onc.2014.333
26. Zhu G, Chen Y, Zhang X, Wu Q, Zhao Y, Chen Y, Sun F, Qiao Y, Wang J (2017) 12-O-Tetradecanoylphorbol-13-acetate (TPA) is anti-tumorigenic in liver cancer cells via inhibiting YAP through AMOT. Sci Rep 7:44940. https://doi.org/10.1038/srep44940
27. Hong SA, Son MW, Cho J, Jang SH, Lee HJ, Lee JH, Cho HD, Oh MH, Lee MS (2017) Low angiomotin-p130 with concomitant high yes-associated protein 1 expression is associated with adverse prognosis of advanced gastric cancer. Apmis 125(11):996–1006. https://doi.org/10.1111/apm.12750
28. Qiu Y, Mao YT, Zhu JH, Zhao K, Wang JF, Huang JM, Chang GQ, Guan YT, Huang FY, Hu YJ, Chen JQ, Liu JL (2021) Correction to: CLIC1 knockout inhibits invasion and migration of gastric cancer by upregulating AMOT-p130 expression. Clin Transl Oncol 23(3):663–4. https://doi.org/10.1007/s12094-020-02495-4
29. Li D, Shen Y, Ren H, Wang L, Yang J, Wang Y (2021) Angiomotin-p130 inhibits vasculogenic mimicry formation of small cell lung cancer independently of Smad2/3 signal pathway. J Bioenerg Biomembr 53(3):295–305. https://doi.org/10.1007/s10863-021-09891-7
30. Sang T, Yang J, Liu J, Han Y, Li Y, Zhou X, Wang X (2021) AMOT suppresses tumor progression via regulating DNA damage response signaling in diffuse large B-cell lymphoma. Cancer Gene Ther 28(10–11):1125–35. https://doi.org/10.1038/s41417-020-00258-5
31. Qiu Y, Mao YT, Zhu JH, Zhao K, Wang JF, Huang JM, Chang GQ, Guan YT, Huang FY, Hu YJ, Chen JQ, Liu JL (2021) CLIC1 knockout inhibits invasion and migration of gastric cancer by upregulating AMOT-p130 expression. Clin Transl Oncol 23(3):514–25. https://doi.org/10.1007/s12094-020-02445-0
32. Lv M, Li S, Luo C, Zhang X, Shen Y, Sui YX, Wang F, Wang X, Yang J, Liu P, Yang J (2016) Angiomotin promotes renal epithelial and carcinoma cell proliferation by retaining the nuclear YAP. Oncotarget 7(11):12393–403. https://doi.org/10.18632/oncotarget.7161
33. Zhang Y, Yuan J, Zhang X, Yan F, Huang M, Wang T, Zheng X, Zhang M (2016) Angiomotin promotes the malignant potential of colon cancer cells by activating the YAP-ERK/PI3K-AKT signaling pathway. Oncol Rep 36(6):3619–26. https://doi.org/10.3892/or.2016.5194
34. Yi C, Shen Z, Stemmer-Rachamimov A, Dawany N, Troutman S, Showe LC, Liu Q, Shimono A, Sudol M, Holmgren L, Stanger BZ, Kissil JL (2013) The p130 isoform of angiomotin is required for Yap-mediated hepatic epithelial cell proliferation and tumorigenesis. Sci Signal 6(291):77. https://doi.org/10.1126/scisignal.2004060
35. Ortiz A, Lee YC, Yu G, Liu HC, Lin SC, Bilen MA, Cho H, Yu-Lee LY, Lin SH (2015) Angiomotin is a novel component of cadherin-11/β-catenin/p120 complex and is critical for cadherin-11-mediated cell migration. Faseb J 29(3):1080–91. https://doi.org/10.1096/fj.14-261594
36. Li S, Yang H, Li W, Liu JY, Ren LW, Yang YH, Ge BB, Zhang YZ, Fu WQ, Zheng XJ, Du GH, Wang JH (2022) ADH1C inhibits progression of colorectal cancer through the ADH1C/PHGDH /PSAT1/serine metabolic pathway. Acta Pharmacol Sin 43(10):2709–22. https://doi.org/10.1038/s41401-022-00894-7
37. Zhang Y, Li J, Dong X, Meng D, Zhi X, Yuan L, Yao L (2020) PSAT1 regulated oxidation-reduction balance affects the growth and prognosis of epithelial ovarian cancer. Onco Targets Ther. https://doi.org/10.2147/ott.S250066
38. Huang SP, Chan YC, Huang SY, Lin YF (2019) Overexpression of PSAT1 gene is a favorable prognostic marker in lower-grade gliomas and predicts a favorable outcome in patients with idh1 mutations and chromosome 1p19q codeletion. Cancers (Basel). 12(1):13. https://doi.org/10.3390/cancers12010013
39. Jiang J, Zhang L, Chen H, Lei Y, Zhang T, Wang Y, Jin P, Lan J, Zhou L, Huang Z, Li B, Liu Y, Gao W, Xie K, Zhou L, Nice EC, Peng Y, Cao Y, Wei Y, Wang K, Huang C (2020) Regorafenib induces lethal autophagy arrest by stabilizing PSAT1 in glioblastoma. Autophagy. https://doi.org/10.1080/15548627.2019.1598752
40. Qian C, Xia Y, Ren Y, Yin Y, Deng A (2017) Identification and validation of PSAT1 as a potential prognostic factor for predicting clinical outcomes in patients with colorectal carcinoma. Oncol Lett 14(6):8014–20. https://doi.org/10.3892/ol.2017.7211
41. Yang Y, Wu J, Cai J, He Z, Yuan J, Zhu X, Li Y, Li M, Guan H (2015) PSAT1 regulates cyclin D1 degradation and sustains proliferation of non-small cell lung cancer cells. Int J Cancer 136(4):E39-50. https://doi.org/10.1002/ijc.29150
42. Zhu S, Wang X, Liu L, Ren G (2022) Stabilization of Notch1 and β-catenin in response to ER- breast cancer-specific up-regulation of PSAT1 mediates distant metastasis. Transl Oncol. https://doi.org/10.1016/j.tranon.2022.101399
43. Jiang J, Li B, He W, Huang C (2021) Dietary serine supplementation: Friend or foe? Curr Opin Pharmacol. https://doi.org/10.1016/j.coph.2021.08.011
44. Biyik-Sit R, Kruer T, Dougherty S, Bradley JA, Wilkey DW, Merchant ML, Trent JO, Clem BF (2021) Nuclear pyruvate kinase M2 (PKM2) contributes to phosphoserine aminotransferase 1 (PSAT1)-mediated cell migration in EGFR-activated lung cancer cells. Cancers (Basel) 13(16):3938. https://doi.org/10.3390/cancers13163938
45. Aase K, Ernkvist M, Ebarasi L, Jakobsson L, Majumdar A, Yi C, Birot O, Ming Y, Kvanta A, Edholm D, Aspenström P, Kissil J, Claesson-Welsh L, Shimono A, Holmgren L (2007) Angiomotin regulates endothelial cell migration during embryonic angiogenesis. Genes Dev 21(16):2055–68. https://doi.org/10.1101/gad.432007
46. Holmgren L, Ambrosino E, Birot O, Tullus C, Veitonmäki N, Levchenko T, Carlson LM, Musiani P, Iezzi M, Curcio C, Forni G, Cavallo F, Kiessling R (2006) A DNA vaccine targeting angiomotin inhibits angiogenesis and suppresses tumor growth. Proc Natl Acad Sci U S A. 103(24):9208–13. https://doi.org/10.1073/pnas.0603110103
47. Troyanovsky B, Levchenko T, Månsson G, Matvijenko O, Holmgren L (2001) Angiomotin: an angiostatin binding protein that regulates endothelial cell migration and tube formation. J Cell Biol 152(6):1247–54. https://doi.org/10.1083/jcb.152.6.1247
48. Huang W, Zeng Z, Xu Y, Mai Z (2023) Investigating whether exosomal miR-205–5p derived from tongue squamous cell carcinoma cells stimulates the angiogenic activity of HUVECs by targeting AMOT. Cancer Biomark 38(2):215–24. https://doi.org/10.3233/cbm-220350
49. Park JA, Kwon YG (2018) Hippo-YAP/TAZ signaling in angiogenesis. BMB Rep 51(3):157–62. https://doi.org/10.5483/bmbrep.2018.51.3.016